

## Enhanced weathering for CO<sub>2</sub> removal using carbonate-rich crushed returned concrete; a pilot study from SE Ireland



Frank McDermott <sup>a,b,c,\*</sup>, Maurice Bryson <sup>d</sup>, Ruadhan Magee <sup>a</sup>, David van Acken <sup>a</sup>

<sup>a</sup> UCD School of Earth Sciences, University College Dublin, Belfield, Dublin, 4, Ireland

<sup>b</sup> Irish Centre for Research in Applied Geosciences (iCRAG), University College Dublin, Belfield, Dublin, 4, Ireland

<sup>c</sup> Earth Institute, University College Dublin, Belfield, Dublin, 4, Ireland

<sup>d</sup> Silicate Ltd, NovaUCD, University College Dublin, Belfield, Dublin, 4, Ireland

### ARTICLE INFO

Editorial handling by: Adrian Bath

#### Keywords:

Enhanced weathering  
Carbon dioxide removal  
Concrete  
Weathering

### ABSTRACT

A 1.21-ha pilot study in SE Ireland investigated crushed returned concrete (CRC), applied at a rate of 7.5 tonnes/ha as a soil amendment for carbon dioxide removal (CDR) by enhanced weathering (EW) over a 10-month period. Most, but not all amended sites showed enhanced concentrations of calcium and bicarbonate in shallow soil waters compared with adjacent controls. Soil pH increased rapidly by 0.3 to >1 pH units ( $5.75 \pm 0.25$  (n = 8) in controls to  $6.5 \pm 0.7$  (n = 24) at amended sites), with greatest increases in soils that had lowest initial pH (<6.0). Aside from one site where concentrations continued to increase, calcium (1.76–0.39 mM Ca) and bicarbonate (4.06–0.64 mM) values in soil waters declined gradually over the course of the study, consistent with rapid initial dissolution and progressive exhaustion of the fine-grained fraction, as indicated by a shrinking-core model. Most sites exhibited high bicarbonate to cation ratios (1.2–2.2) consistent with CRC dissolution by soil carbonic acid, although two sites adjacent to the field-boundary river that floods periodically showed evidence for strong acid (nitric) dissolution. Enhanced bicarbonate levels in soil waters at amended sites compared with controls, coupled with a downward-flush hydrological model driven by annual effective rainfall to calculate bicarbonate export and a simple stoichiometric correction for nitric acid weathering, indicate gross CDR rates in the range zero to 0.52 tonnes CO<sub>2</sub>/ha (69 kg CO<sub>2</sub>/tonne), limited by bicarbonate export rather than weathering rates. Further optimisation of the CDR efficiency of this material should be possible using strategies to avoid or pre-neutralise non-carbonic soil acids and by taking account of sub-aerial carbonation at the post-crushing, pre-amendment stage that arises when the material is crushed in preparation for EW applications. A simplified life-cycle analysis indicates that a discount of about 11% should be applied to account for CO<sub>2</sub> emissions from crushing, transport and spreading operations.

### 1. Introduction

The imperative for large-scale carbon dioxide removal (CDR) from the atmosphere to achieve 'net zero' targets by mid-century is well understood (Fuss et al., 2014; IPCC et al., 2021). Recently, there has been renewed interest in enhanced weathering (EW) of crushed rocks, minerals and alkaline wastes for CDR. Enhanced weathering approaches are attractive because of their scalability, low capital cost and broad alignment with circular economy goals (Hartmann et al., 2013; Renforth, 2012, 2019; Beerling et al., 2020; Goll et al., 2021). The premise is that weathering rates of minerals and rocks can be enhanced by adding them as finely crushed powders to soils, where they are weathered by

carbonic acid, generated when soil-gas CO<sub>2</sub> dissolves in downward percolating soil water. The high pCO<sub>2</sub> of soil gases that drives carbonic acid formation arises predominantly from plant root respiration and natural decomposition of soil organic matter. If successful, enhanced weathering approaches for CDR should result in a reduction of the current large natural diffusive efflux of CO<sub>2</sub> from soils to the atmosphere ( $68 \pm 4$  Pg CO<sub>2</sub> yr<sup>-1</sup> globally; Raich and Schlesinger, 1992) by conversion of carbonic acid to relatively stable dissolved bicarbonate ions, which are ultimately transported to groundwater systems (Gastmans et al., 2016) and to the oceans. A co-benefit of increasing the alkalinity of stream and river waters is that existing rates of natural CO<sub>2</sub> evasion from these surface waters may be reduced.

\* Corresponding author. UCD School of Earth Sciences, University College Dublin, Belfield, Dublin, 4, Ireland.

E-mail address: [frank.mcdermott@ucd.ie](mailto:frank.mcdermott@ucd.ie) (F. McDermott).

Critically, it is important not to conflate weathering and CDR. The distinction is essential because weathering in soils can be driven by acids other than carbonic acid, particularly in anthropogenically impacted systems (Perrin et al., 2008). Demonstration that dissolved bicarbonate ion loads are higher in the soil pore waters of amended soils compared with those from adjacent control plots is essential to provide robust evidence for carbonic acid driven mineral weathering, and therefore CO<sub>2</sub> drawdown. Ultimately, some fraction of the weathering-generated bicarbonate ion load is transported to the oceans via surface drainage and groundwater pathways; the latter including direct sub-marine freshwater exports to the oceans via the continental shelves. Once transported to the oceans, bicarbonate ions have an average residence time of c. 80,000 years (Berner and Berner, 1987), leading to a net removal of inorganic carbon from the atmosphere to the oceans on centennial to millennial timescales. From a CDR perspective, this provides a degree of permanency that is useful in the context of the current climate emergency, regardless of the ultimate fate of oceanic bicarbonate on geological timescales.

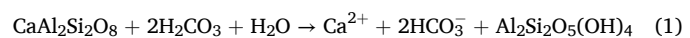
Until recently, many studies of enhanced weathering for CDR have adopted a high-level theoretical or techno-economic modelling approach, generally based on proposals to use crushed mafic rocks (e.g. basalt) and ultramafic minerals such as olivine as soil amendments (Strelfer et al., 2018; Andrews and Taylor, 2019; Haque et al., 2019; Beerling et al., 2020; Goll et al., 2021; Lewis et al., 2021; Kantzas et al., 2022; Baek et al., 2023). Several studies have employed theoretical mineral dissolution rates from laboratory-based studies to estimate weathering rates (Strelfer et al., 2018; Lewis et al., 2021; Baek et al., 2023), but laboratory experiments are generally conducted in well-mixed reactors that are known to overestimate field weathering rates (Paces, 1983; White and Brantley, 2003; Wild et al., 2019). To better assess field-relevant conditions, some studies have employed mesocosm experiments as a ‘halfway-house’ between laboratory- and field-scale experiments (Buckingham et al., 2022; ten Berge et al., 2012; Kelland et al., 2020), but there have been relatively few reports from hectare-scale in-situ field deployments of rock powders for EW-CDR in agricultural settings (Haque et al., 2020; Taylor et al., 2021; Larkin et al., 2022; Kantola et al., 2023).

The objective of this study is to present ‘proof of concept’ results from a hectare-scale pilot field experiment. Unlike previous studies that generally deploy basalt or olivine as the soil amendment material, we have investigated the use of an abundant surplus industrial alkaline material (crushed returned concrete; CRC) as a potential soil amendment for CDR. CRC is produced by crushing solidified returned concrete, a surplus alkaline product of the ready-mix concrete industry globally. In Ireland CRC is classified as a surplus product, not a waste material, although we are mindful that classification may vary in different countries. Globally, it is estimated that returned concrete comprises 1–4% of all concrete produced, depending on jurisdiction (Ren et al., 2022; Xuan et al., 2016). Global concrete production is estimated at 25 billion tonnes (Ren et al., 2022), which implies returned concrete supplies of 250–1000 million tonnes/year, implying a widely distributed material that could be re-purposed for CDR.

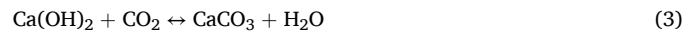
A typical mix in CRC would be three parts coarse aggregate, two parts sand (both limestone in this case) and one part Portland cement. Approximately 1–4% of ready-mix concrete produced globally is returned undelivered to point-of-origin mixing plants (Xuan et al., 2016; Ren et al., 2022) on a global basis, for a variety of reasons (e.g. the concrete fails to meet customer specifications, excess concrete ordered to ensure complete same-day concrete pours on large construction sites). Unlike construction and demolition waste, CRC is a virgin product and is free from potentially harmful building-related contaminants (e.g. asbestos, insulation fibres) that can occur in construction and demolition (C & D) waste. In many jurisdictions, returned concrete is coarsely crushed only before burial as a low-value fill material (e.g. road base) in construction sites. As described below, the CRC material utilised here is essentially free of contaminants that can occur in olivine and to a lesser

extent in basaltic soil amendments (e.g. Ni, Cr). Returned concretes containing other rock types as aggregates (e.g. igneous or metamorphic rocks) could also be used as a material for CDR, but each material would require investigation in terms of its weathering efficacy and any possible detrimental effects.

Simplified generic geochemical reactions that are relevant have been presented previously (Hartmann et al., 2013). Briefly, when silicate rock and minerals are weathered by carbonic acid, 2 mol of atmospheric CO<sub>2</sub> (as dissolved bicarbonate) are sequestered per mole of released bivalent cations such as Ca, Mg. For reference, reaction 1 below is an example of a calcium-bearing silicate mineral (anorthite) undergoing weathering by reaction with carbonic acid to release calcium and bicarbonate ions into soil solutions. In this case, both moles of the resulting bicarbonate carry carbon that was originally present as soil CO<sub>2</sub>. This contrasts with weathering of a carbonate mineral (e.g. calcite) in which only one of the 2 mol of bicarbonate produced carries carbon from soil CO<sub>2</sub>; the other being limestone-derived. Reaction 2 below is relevant for the current study, because limestone rock aggregate forms a high proportion of the CRC amendment material utilised here.

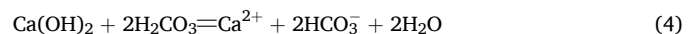


However, alkaline materials such as CRC also contain variable amounts of Ca(OH)<sub>2</sub> (portlandite) that arises from CaO (lime) hydration when concrete is manufactured. The cement paste component of concrete, typically 20–25% by mass, depending on cement: aggregate ratios, initially contains approximately 20% portlandite by mass (von Greve-Dierfeld et al., 2020). Over time, portlandite becomes carbonated by reacting directly with atmospheric CO<sub>2</sub> in the presence of moisture to produce secondary calcium carbonate (reaction 3), but the rate of carbonation is highly dependent on grain size and moisture availability. In uncrushed concrete this carbonation process is sluggish (decades to centuries depending on surface area/mass ratios), limited by slow inward diffusion of atmospheric CO<sub>2</sub> (Pade and Guimaraes, 2007).



This CO<sub>2</sub>-sequestering reaction is expected to occur rapidly under sub-aerial conditions after concrete is crushed and milled to manufacture CRC, compared with background rates of carbonation that would occur if the same material was left largely uncrushed or in centimetre to decimetre-scale fragments in stockpiles, as discussed below.

When CRC is added to soils, in the presence of soil carbonic acid, any residual non-carbonated portlandite that survives the post-crushing/pre-spreading sub-aerial carbonation stage can react further to remove CO<sub>2</sub> as follows:



As in reaction 2, 2 mol of bicarbonate are produced per mole of calcium released to the water, but an important distinction is that reaction 4 is more efficient for CDR because both moles of the produced bicarbonate contain carbon from atmospheric CO<sub>2</sub>. Notwithstanding the likelihood that some carbonate in the CRC material might have been produced by sub-aerial carbonation of portlandite (reaction 3) during post-crushing/pre-spreading storage, it is conservatively assumed in CDR calculations below that only 50% of the observed enhanced bicarbonate in the soil waters of our amended sites is atmospheric in origin (reaction 2).

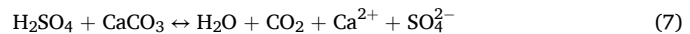
When dissolved bicarbonate is transported to the oceans and eventually combines with dissolved cations (e.g. Ca<sup>2+</sup>, Mg<sup>2+</sup>) in seawater to precipitate marine limestones on geological timescales, half of the CO<sub>2</sub> consumed by silicate weathering and all of the CO<sub>2</sub> consumed by limestone weathering is released back to the atmosphere (reaction 5).



Thus, ocean-evaded CO<sub>2</sub> that accompanies limestone precipitation in the oceans on geological timescales eventually negates 50% of the ‘weathering consumed’ CO<sub>2</sub> by silicate weathering, and all ‘weathering consumed’ CO<sub>2</sub> in the case of carbonate weathering. For this reason, it has long been argued that on geological timescales, weathering of carbonate lithologies such as limestones is neutral with respect to atmospheric CO<sub>2</sub> (Berner and Berner, 1987). Importantly however, the disadvantage of limestone weathering as a CO<sub>2</sub>-consuming reaction can be neglected if the CDR goal is to reduce atmospheric CO<sub>2</sub> on the short (centennial to millennial timescales) that are relevant to the current climate emergency. This arises because the relatively long (c. 10<sup>5</sup> year) residence time of bicarbonate ions in seawater exceeds the mixing times of the oceans and enhanced transfer of dissolved bicarbonate to the oceans constitutes an effective additional CO<sub>2</sub> sink. Indeed, some authors (e.g. Zheng et al., 2022) have advocated liming as a global atmospheric CDR strategy, providing that suitable carbonate-undersaturated river systems can be chosen to avoid CO<sub>2</sub> losses as a result of secondary carbonate precipitation within drainage basins or soils (Knapp and Tipper, 2022). Precipitation of secondary carbonates (e.g. pedogenic carbonates in soils, tufas or similar deposits in streams or rivers) by CO<sub>2</sub> degassing at any point enroute from the site of soil weathering to the oceans would cancel out any atmospheric carbon dioxide removal by carbonate rock weathering, and halve the CO<sub>2</sub> drawdown efficacy of silicate weathering. Pedogenic carbonates are likely to be ephemeral in non-alkaline soils in humid regions and later carbonic-acid driven dissolution could re-sequester the CO<sub>2</sub> temporarily lost by carbonate precipitation. Based on global occurrence, pedogenic carbonate formation and preservation is linked to hyperarid, arid and semi-arid climates (Cerling, 1984; Plaza et al., 2018), although more research is needed to better constrain their longevity in seasonally dry and semi-arid conditions. Based on aridity indices globally, Plaza et al. (2018) have estimated that hyperarid, arid and semi-arid regions together account for approximately 30% of the global land area and calcisols (soils with secondary calcium carbonates) account for 7.4%, 16.9% and 5.76% of the land areas in these regions respectively, with negligible occurrences in dry and humid regions. Overall, calcisols are estimated to account for 4.2% of the global land area. A cautious approach would be to ensure that bicarbonate-receiving waters (soil waters and surface drainage waters) remain undersaturated with respect to carbonates by limiting amendment application rates, taking factors such as water pH, temperature as well as meteorological variables such as potential evapotranspiration and effective rainfall into account.

A more serious challenge for the use of limestone or other carbonate-rich lithologies as soil amendments for CDR is that CO<sub>2</sub> gas could be produced if non-carbonic acids (e.g. strong acids such as HNO<sub>3</sub> or H<sub>2</sub>SO<sub>4</sub>) are involved in the weathering process (Perrin et al., 2008; Knapp and Tipper, 2022). Avoiding this problem requires careful selection of sites as well as monitoring of bicarbonate concentrations and bicarbonate/cation molar ratios in soil waters, as well as assessment of soil-to-atmosphere CO<sub>2</sub> fluxes. Strong acids can also impact the efficacy of silicate mineral-based EW, particularly if soil pCO<sub>2</sub> is low (Dietzen and Rosing, 2023), and the silicate material contains minor secondary carbonates, particularly if high amendment rates (e.g. > 25 tonnes/ha) are used for silicate-rock enhanced weathering schemes (Beerling et al., 2020; Kantola et al., 2023). Acidity arising from nitrogenous fertiliser use (e.g. proton production by nitrification of ammonium) probably poses a greater challenge than sulphuric acid (e.g. from atmospheric SO<sub>2</sub> deposition or from minor amounts of pyrite in rock amendments), because of the widespread use of nitrogenous chemical fertilisers in intensively farmed agricultural soils. Critically, neither of the exemplar ‘strong acid’ driven carbonate weathering reactions below (6 & 7) produce the requisite dissolved bicarbonate ions in soil waters, and instead produce rather than sequester CO<sub>2</sub>, highlighting the risks inherent in the use of carbonate-bearing soil amendments in soils that may contain strong acids, and the need to carefully assess the fraction of minor secondary carbonates in some meta-basalts and other silicate

amendments (Kemp et al., 2022).



Notwithstanding these potential risks, an important advantage of carbonate lithologies as soil amendments for CDR is that their dissolution kinetics are orders of magnitude faster compared with silicate rocks and minerals (Liu et al., 2011; Hartmann et al., 2013; Knapp and Tipper, 2022; Zheng et al., 2022). These considerations are relevant for the current study, because the crushed returned concrete amendment employed here contains limestone as the aggregate rock, in addition to small amounts of surviving partially carbonated hydroxides such as portlandite and artificial cementitious calcium silicate hydrates (CSH). Protons released by strong acid dissociation are expected to react with residual (uncarbonated) portlandite (Ca(OH)<sub>2</sub>) to produce calcium ions and water, and release nitrate or sulphate ions to the water for nitric and sulphuric acid systems respectively.

## 2. Field study site

The field trial comprised a 1.21 ha (c. 3 acre) field in Co. Wexford, SE Ireland that is cultivated annually to grow mixed seed crops (barley, oats, linseed) as Wild Bird Cover under Teagasc’s (Irish Agricultural Advisory Agency) GLAS Scheme (hereafter the BF site), centred on 52°19'11"N, 6° 50'24"W (Fig. 1). The CRC amendment was applied once on June 7th 2021 using a tractor-drawn lime spreader at a nominal rate of 7.5 tonnes/ha, although spatial variability in the application rate was unavoidable, particularly around the edges of the field. The amendment was mixed into the upper 15–20 cm of the soil by the no-plough minimum tilling seed-sowing operation in the days following spreading. A c. 30 m-wide strip through the centre of the field was left unamended as a control area, but was otherwise subject to the same agricultural operations as the remainder of the field. No chemical or organic fertilisers were applied over the course of the study and the site has had a history of low-intensity management over several years to comply with the GLAS Scheme conditions.

The soils are well drained and have a loam to clay-loam texture with abundant shale fragments and are classified as Brown Earths (Gardiner and Ryan, 1969). The area is underlain by Ordovician shales and slates of the Campile Formation and was glaciated during the Last Glacial Maximum (Hughes et al., 2016). The soils are limestone-free silty clay loams, having developed on glacial till containing abundant shale and slate lithic fragments from the underlying bedrock. The soils are free-draining but the north-east margin of the field is subject to periodic seasonal flooding from the adjacent river (Fig. 1) and this occurred at sites BF3 and BF8 briefly during spring 2022.

SE Ireland has a cool temperate climate with a mean annual air temperature (MAAT) of 10.4°C. Meteorological data from Met Éireann’s (Ireland’s meteorological service) synoptic station at Johnstown Castle, 23 km east of the study area were used along with monthly potential evapotranspiration (PET) estimates derived by Met Éireann using a modified Thornthwaite method for the years 2020, 2021 and 2022 (<https://www.met.ie>).

## 3. Methods

### 3.1. Soil waters

To monitor changes in shallow soil water chemistry attributable to weathering of the CRC material, eight Soil Moisture Corporation® porous ceramic-cup soil water samplers were installed at the BF site on June 12, 2021, five days after application of the amendment. All samplers were 40 cm long, apart from those at the BF2 and BF7 which were 25 cm long, but all were installed to ensure that the critical porous cup part of each sampler was 15–20 cms below the soil surface. Of the eight



**Fig. 1.** Location of the BF study site in SE Ireland and locations of the eight ceramic-cup soil water samplers deployed in the 1.21 ha field. Locations 4 and 5 are the control sites. The Owenduff River runs along the northern and north-eastern boundaries of the field.

soil-water samplers deployed, six were sited on parts of the field that had been amended with the CRC (BF1, BF2, BF3, BF6, BF7, BF8) and the remaining two (BF4 & BF5) were deployed in the unamended control strip (Fig. 1).

Soil waters were generally retrieved monthly from the samplers in the period July 2021 to April 2022, although no water could be retrieved at some locations during summer 2021. Following return of the water samples to the UCD lab they were stored at 4°C. Water pH measurements were generally completed within 24 h. Electrical conductivity was analysed on filtered non-acidified soil water samples following probe calibration using standard solutions. Within 48 h of sample collection, total alkalinity (TA) in the waters was measured by titration in the presence of a mixed methyl red/bromocresol green indicator against 0.08M H<sub>2</sub>SO<sub>4</sub> Hach®, dispensed dropwise using a manual digital titrator.

Aliquots of the water samples were filtered using 0.45 µm cellulose filters prior to acidification to yield 3% nitric solutions for major and trace element (cation) analyses using a ThermoFisher Scientific iCAP-Q inductively coupled plasma mass spectrometer (ICP-MS) in collision cell mode at the National Centre for Isotope Geochemistry (NCIG) at the School of Earth Sciences, University College Dublin, using He with a flow of 4.85 ml/min as the collision gas. The instrument was calibrated using a multielement mixed standard (SigmaAldrich TraceCert® Periodic Table Mix 1), diluted to give a range of different concentrations. Calcium concentrations in water samples were measured separately and standardized with a mono-element Ca standard solution to circumvent isobaric interference by doubly charged <sup>88</sup>Sr. Monitored masses were <sup>23</sup>Na, <sup>24</sup>Mg, <sup>27</sup>Al, <sup>39</sup>K, <sup>43</sup>Ca, <sup>44</sup>Ca, <sup>47</sup>Ti, <sup>48</sup>Ca, <sup>52</sup>Cr, <sup>56</sup>Fe, <sup>60</sup>Ni, <sup>88</sup>Sr, and <sup>137</sup>Ba, with 10 sweeps/run, 20 runs/sample, and dwell times of 10 ms for Na, Mg, and K, 50 ms for Ca, and 20 ms for all other masses. Major elements such as Ca, K, and Na were determined on diluted samples, while trace elements were analysed without dilution. Analytical in-run precision is typically between 1 and 2% for all reported elements. Detection limits are conservatively estimated at 0.01 ppb for Cr, Ni, Sr, and Ba, below 0.1 ppb for Fe, below 0.2 ppb for Na and Mg, below 0.5 ppb for Al, and below 2 ppb for Ca and K and are estimated by the ThermoFisher Scientific iCAP-Q Qtegra software using the formula given in the caption of Table S6. Accuracy of the ICP-MS trace element analyses were assessed by multiple analysis of the Canadian Reference Material SLRS-6-CRM (River water standard) and representative analysis are given in Table S6. Blanks were negligible, and no blank corrections were applied.

Anion concentrations were analysed on 0.45 µm filtered non-acidified aliquots of the soil-water samples using a Metrohm ion-

chromatography instrument at UCD, following standardisation using certified Merck Sigma Aldrich® multi-anion standard solutions. All samples were analysed for fluoride, chloride, bromide, nitrate, phosphate and sulphate, although some analytes were below detection limits (0.1 ppm) in several samples. Accuracy was assured by measuring one vial containing an independent (Merck Supelco®) certified reference material (Multi Anion Standard 1 for IC) as an unknown in every batch of 12 unknown samples. This quality assurance standard is independent of the Merck standard solutions (Multi Anion Standards 2 and 3 for IC) that were used for calibration curve construction by the Metrohm software. All Merck standard solutions are traceable to NIST SRMs or similar CRMs. Long-term data for the quality assurance standard (*n* = 21) are presented in Table S7. Blanks were negligible and no blank corrections were applied.

Geochemical speciation modelling and saturation-state evaluation was carried out for each soil water using the interactive version of PHREEQC (Parkhurst and Appelo, 1999) at 10°C based on the MINTEQ thermodynamic database. Prior to use, the MINTEQ thermodynamic database was modified to include data for cementitious minerals relevant to this study such as portlandite using the Cemdata18 database of Lothenbach et al. (2019). PHREEQC geochemical modelling was also used to investigate the upper limits of soil-water dissolved bicarbonate and calcium concentrations imposed by calcite saturation as a function of water pH.

### 3.2. Soil characterisation

Soil samples (c. 500g) were taken from an area within a 1m radius of each of the eight soil water samplers on four occasions during the study (June 2021, October 2021, January 2022 and April 2022) using a 15 cm soil auger. pH measurements were completed in triplicate on each sample using 15 g of moist soil, suspended in 30 mls of deionised (18.2 MΩ) water using a calibrated (pH 4, 7, 10) pH probe. The mean result is reported in all cases. The external precision of pH measurements on different soil aliquots of the same sample bag is generally better than 0.1 pH units.

The soil samples collected on October 16th 2021, approximately 4 months after amendment application, were also subjected to leaching experiments to estimate the extent to which weakly-bound soil exchangeable calcium had increased in the amended compared with the control soils. These samples were leached in duplicate using a 0.03M NaCl solution (2g of soil in 10 mls of solution) following the 2-h leaching protocol of ten Berge et al. (2012). The supernatant solutions were

analysed for Ca by ICP-MS analysis following centrifugation and filtration ( $0.45\text{ }\mu\text{m}$ ).

To evaluate spatial variability in amendment application rates and to aid with the interpretation of the soil-water geochemical data, aliquots of soils from sites BF1–BF8 sampled 7 months after the amendment was applied (Jan 2022) were analysed for strong-acid (1M HNO<sub>3</sub>) soluble calcium. One gramme of 105 C° oven-dried aliquots of soil was strongly leached overnight in 25 mls 1M HNO<sub>3</sub> to completely dissolve the carbonate fraction as well as any residual portlandite and calcium silicate hydrate phases and to remove exchange-site bound soil calcium. Following centrifugation and 100x dilution, the solutions were analysed for calcium by ICP-MS.

### 3.3. Amendment material characterisation

XRD, XRF and grain size distribution measurements were carried out on a single sample after obtaining a representative sample by cone-and-quartering. The grain size distribution of the CRC amendment was determined by gravimetric sieve analysis following dry sieving using a stack of wire sieves (2 mm–63 µm) on a motorized sieve shaker. Quantitative X-ray diffraction (XRD) analysis for mineralogical characterization of the CRC material was completed by Actlabs (Ontario, Canada). Pulverized samples were mixed with corundum as an internal standard. A Bruker D8 Endeavour XRD instrument equipped with a Cu X-ray source was used and mineral identification was based on the PDF4/Minerals ICDD database. The Rietveld method was used to determine the quantities of the crystalline mineral phases and the remainder after summation to 100% was reported as amorphous material.

Prior to deployment of the CRC material as a soil amendment, its pH was measured using a 2:1 mass ratio of CRC material to deionised water, similar to the protocol described above for soil pH measurement. Major element and selected trace element contents of the CRC material and a sample of typical Irish ground agricultural limestone were determined by ICP-OES following a 4-acid digestion method of fused powder at Actlabs (Ontario, Canada). Detection limits are 0.01 wt% for all major element oxides except for MnO and TiO<sub>2</sub> (0.001 wt%). A range of standards and geochemical reference materials (NIST 694, DNC-1, SY-4, BIR1a, W-2b) were analysed to ensure quality control of the dissolution process and accuracy of the analytical data (Table S8). Hexavalent chromium was additionally measured in the material following US EPA Methods 3060A (alkaline digestion, 2 ppm detection limit), followed by reaction with diphenylcarbazide and colorimetric measurement at 540 nm (Method 7196A) at Eurofins laboratory, Pensacola, Florida.

The specific surface area (m<sup>2</sup>/g) of the CRC amendment was measured by BET gas (N<sub>2</sub>) adsorption by Intertek Wilton Ltd (UK) using a Micromeritics Ltd Tristar II Plus Nitrogen adsorption instrument. Samples were loaded into clean, dry, tared specimen tubes. The sample was degassed under vacuum for 10 min followed by 4 h at 120 °C ± 5 °C until a stable vacuum reading was achieved and was then cooled under vacuum and weighed to obtain the mass of sample tested (2.703g). The resulting 11-point BET plot of  $(1/[Q(p^0/p-1)])$  vs. relative pressure ( $p/p^0$ ), where Q is the quantity of gas adsorbed, was strongly linear (correlation coefficient: 0.99984, p value < 0.001).

### 3.4. Rainfall and potential evapotranspiration

Data from Met Eireann's synoptic station at Johnstown Castle (23 km east of study site) includes all major parameters such as monthly rainfall and evapotranspiration (<https://www.met.ie/climate/available-data>). More restricted datasets (monthly rainfall amounts) are also available from the local Met Eireann meteorological station at Foulksmills (6 km east of study site) for the period of interest. The long-term (30 year) average rainfall at Foulksmills is  $1060 \pm 52$  mm, with annual rainfall of 1097, 1078 and 1047 mm respectively for the calendar years 2020, 2021 and 2022, similar to values of 1150, 1068 and 997 mm for these years at

the synoptic Johnstown Castle station. Annual precipitation minus potential evapotranspiration values were used to estimate soil-water throughput fluxes that were in turn used to calculate bicarbonate fluxes for carbon dioxide removal calculations as described below. Potential evapotranspiration values, calculated by Met Eireann are available for the Johnstown Castle station (557, 542 and 575 mm respectively for 2020, 2021 and 2022), leaving a residual 'effective rainfall' of 593, 526 and 422 mm for these years. To calculate annual water fluxes through the soils, a mean 'effective rainfall' value of  $514 \pm 86$  mm was used (mean ± 1 standard deviation for the rainfall minus evapotranspiration for the years 2020–2022).

## 4. Results

### 4.1. Characterisation of CRC amendment

#### 4.1.1. Grain size distribution and specific surface area

Dry sieving of the supplied <4 mm CRC material produced the grain size distribution data illustrated in Fig. S1. Approximately 76% (by mass) of the material is finer than 2 mm, 55% is finer than 1 mm and 20% is finer than 0.25 mm. The material currently does not meet the EU grain size specifications for ground agricultural limestone (EU, 2019) which stipulates that >70% should be finer than 1 mm. The specific surface area of the CRC material estimated by BET gas-adsorption techniques (Brunauer et al., 1938) described above was relatively high ( $10.6 \pm 0.57$  m<sup>2</sup>/g (mean of 2 measurements on separate aliquots ± 2 standard deviations; Table S1).

#### 4.1.2. CRC amendment pH

As expected, the CRC material is highly alkaline. pH measurements on 2:1 deionised water:solid suspensions yielded values of  $12.40 \pm 0.02$  (n = 3). The chosen application rate (7.5 t/ha) corresponds to a mass ratio of approximately 0.0056 (amendment/soil) assuming a CRC density of 2.4 g/cm<sup>3</sup>, a soil bulk density of 1.33 g/cm<sup>3</sup> and a 10 cm mixing depth.

#### 4.1.3. Mineralogical and major element composition

Table 1 shows quantitative XRD mineralogical data for a single sample of the CRC material. The material is dominated by calcite, largely from the Mississippian limestone from Belgard Quarry in Co. Dublin that forms the major aggregate in this concrete, with minor dolomite. Non-crystalline amorphous material comprises almost 8% by weight. Small quantities of the phyllosilicate minerals illite and chlorite are also present. Overall, the chemistry and mineralogy of this CRC is dominated by the limestone aggregate, but the low portlandite content estimated by XRD compared with many freshly cured concretes (von Greve-Dierfeld et al., 2020) may reflect sub-aerial post-crushing carbonation to calcite and/or under-representation of the portlandite in the XRD results because some portlandite can be in amorphous form that is not recorded by XRD (Keppert et al., 2021). Almost 14% of the material is identified by XRD as quartz which is likely to remain inert during weathering.

Major element data, expressed as wt % oxides on a dry-weight basis are shown in Table 2. The material is highly calcareous, consistent with its high calcite content. The high loss-on-ignition (LOI) value (33.24 wt %) is ascribed primarily to CO<sub>2</sub> loss. It is noteworthy that calcium and carbon molar percentages in the material are very similar (0.774 vs. 0.755 Mol. % respectively) if the assumption is made that all measured LOI is due to CO<sub>2</sub> loss. The slight excess of Ca over C permits up to about 1.5 w% of other non-carbon bearing calcium-rich phases such as residual portlandite and calcium silicate hydrate gels, but the nearly identical molar percentages of Ca and C underline the dominance of calcite.

For the silica budget, a quartz (SiO<sub>2</sub>) content of 13.70 wt% measured by quantitative XRD (Table 1) can account for most (79%), but not all the 17.32 wt % SiO<sub>2</sub> measured by ICP-OES (Table 2). Minor amounts of the remaining 3.62 wt % silica can be accommodated within silicates

**Table 1**

Mineralogy (w %) of the CRC material measured by quantitative XRD on a dry-weight basis. Note that the 7.9 wt% value for ‘amorphous’ is simply the difference between the wt% sum of the crystalline minerals determined by XRD and 100%. \*Ettringite may include thaumasite. Relative errors in quantified wt% values are up to 20%.

Quartz	Illite	Chlorite	Calcite	Dolomite	Hydrotalcite	Portlandite	Ettringite*	Amorphous
13.70	1.0	0.3	71.1	3.5	1.3	0.8	0.4	7.9

**Table 2**

Major element data for the CRC material recalculated on an oxide basis from the elemental concentrations determined by ICP-OES analysis after nitric acid digestion of lithium metaborate/lithium tetraborate fused beads.

SiO <sub>2</sub>	Al <sub>2</sub> O <sub>3</sub>	Fe <sub>2</sub> O <sub>3</sub>	MnO	MgO	CaO	Na <sub>2</sub> O	K <sub>2</sub> O	TiO <sub>2</sub>	P <sub>2</sub> O <sub>5</sub>	LOI	Total
17.32	2.03	1.10	0.152	1.46	43.41	0.10	0.40	0.12	0.05	33.24	99.38

minerals, with some of the remaining Si likely hosted by non-stoichiometric di- and tri-calcium silicate hydrate (CSH) gels from the cementitious component of the CRC, consistent with its relatively high non-crystalline amorphous component (7.9 wt %), (Table 1).

#### 4.1.4. Metal contents of the CRC amendment

The potential impact of soil amendments on the metal content of agricultural soils is an important consideration when selecting amendments for CDR by enhanced weathering. Concerns have been expressed regarding nickel and chromium in the case of olivine and ultramafic rock-based soil amendments (Hartmann et al., 2013; Andrews and Taylor, 2019). Since the CRC material is not an igneous rock, there is no reason to suspect that these elements would be present in elevated concentrations. While trace metal contents are higher than in a typical agricultural ground limestone, Ni, Hg, Pb, As, Cu and Zn values remain 4 to 12 times lower than the EU limits for liming materials (Table 3; EU, 2019).

The Ni content of the CRC is 12 ppm (Table 3), one to two orders of magnitude lower than that of olivine which is typically in the range 130–4900 ppm depending largely on its forsterite ( $Mg_2SiO_4$ ) content (Barnes et al., 2023; ten Berge et al., 2012; Flipkens et al., 2021). The Ni content of the CRC is markedly lower than in basalts (18–200 ppm; Lewis et al., 2021). Estimates for the average Ni content of mid-ocean ridge basalts for example range from 92 to 200 ppm (Gale et al., 2013; Arevalo and McDonough, 2010).

Total chromium in the CRC (10.6 ppm, Table 3) is also much lower than in basalts (35–350 ppm; Lewis et al., 2021), with an average Cr content of 250–320 ppm in mid-ocean ridge basalts (McDonough, 1994; Arevalo and McDonough, 2010; Gale et al., 2013). Total chromium is also markedly lower than in olivine (up to 68–2383 ppm; Flipkens et al., 2021). Hexavalent chromium, a known carcinogen is potentially a concern for concrete-based soil amendments because oxidation of chromium in cement kiln feedstock materials is known to occur (Estokova et al., 2018), and can be released by weathering of the cementitious component of concretes (Keppert et al., 2021) where it can form a soluble oxyanion in waters. In the CRC, hexavalent chromium levels were below the 2 ppm detection limit of the alkaline digestion/colourimetric method utilised which is also the limit for liming materials in the EU regulations (Table 3).

#### 4.2. Soils

##### 4.2.1. Soil pH

At the amended sites, soil pH values are typically 0.3–1.1 pH units higher compared with the control sites (Table S2; Fig. 2). At the two control sites (BF4 and BF5) soil pH values vary by approximately  $\pm 0.25$  pH units through the study, but clearly remain lower than at all six amended sites (Fig. 2). Taken as a group, soil pH values ( $n = 24$ ) at all six amended sites are statistically different from all unamended (control) group ( $n = 8$ ) with averages of 6.48 and 5.7 respectively (Welch Two

**Table 3**

Trace metals in various proposed soil amendments and ground agricultural lime. Metals listed in the upper part of the table are those specified in the EU liming material regulations (EU 2019). Elements listed in the lower part of the table are not specified in the liming regulations but were analysed for completeness. The values shown in parentheses in the upper left-hand column are the maximum allowable levels for liming material specified in EU regulations. The values in the second and third columns respectively are our analyses of CRC and of a typical agricultural ground limestone used in Ireland for comparison. Values in parentheses in the middle column are ranges for metals in agricultural ground limestone where available from the literature (Morris et al., 2000; McBride and Spiers, 2001; Gabe and Rodella, 1999). The right-hand column, for reference, are values for mid-ocean ridge (MORB) basalts from the compilation of Gale et al. (2013) and the values of Russell et al. (2021) were used for arsenic. Estimates for Cd and Hg contents of basalts are from Yi et al. (2000) and Coufalik et al. (2018) respectively. Basalt values vary greatly depending on type, with elements that are incompatible in magmatic systems (e.g. Ba) showing values up to several hundred ppm in some alkalic basalts. n.a. = ‘not analysed’ (lime) or ‘not available’ (Cd and Hg in basalt).

EU regulation trace metal limits for liming material	CRC (mg/kg)	Ground Agricultural Lime(mg/kg)	Basalt* (mg/kg)
Cd (2 ppm)	<0.4	<0.4 (<0.1–1.1)	0.1–0.13
Hexavalent Cr (2 ppm)	<2	<2	<2
Hg (1 ppm)	<0.20	<0.20 (<0.01–0.02)	<0.0005
Ni (90 ppm)	11.7	5.0 (7–17)	92
Pb (120 ppm)	23.7	3.0 (1.3–130)	0.57
As (40 ppm)	10.6	2.36 (<1–3)	<1 to 11
Cu (300 ppm)	31.6	2.2 (3–21)	74
Zn (800 ppm)	64.7	<3.0 (5–113)	91.3
<b>Other metals</b>			
Cr (total)	10.6	3.61 (<10)	249
U	0.81	0.31	0.12
Ba	342	(<10–1265)	29
Sr	290	n.a.(36–4736)	129
Y	11	n.a.	37
Sc	3	n.a.	40
Zr	34	n.a.	117
V	28	n.a.	309

Sample *t*-test  $p = <0.001$ . pH increases markedly in the four months between initial spreading of the material in early June 2021 to October 2021 and then increases at a lower rate or remained relatively constant until the third soil sampling event in late January 2022. Values decrease again or increase only slightly until the final soil sampling event on April 1st 2022. For each of the four sampling intervals (June 2021, October 2021, January 2022 and April 2022), the pH of soils at amended sites are always higher at the 95% confidence level compared with the contemporaneous control sites (Welch Two Sample *t*-test  $p$  values  $< 0.001$  all months).

The effect of the CRC amendment on soil pH was rapid. The first batch of soil samples taken on June 12th 2021, seven days after

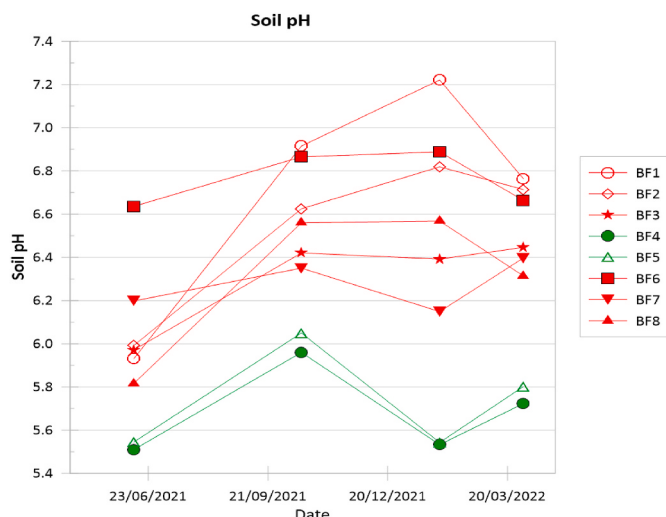


**Fig. 2.** Evolution of soil pH during the study. Sites BF4 and BF5 are unamended controls. Typical analytical errors are 0.05 pH units.

amendment application show elevated pH relative to the controls, suggesting the presence of a relatively soluble high-pH component in the CRC. As a group, the pH values of the June 2021 amended soils are lower at the 95% confidence level compared with values from all subsequent three sampling intervals with Welch Two Sample *t*-test *p* values < 0.001, < 0.05 and < 0.05 for the October, January and April samples respectively. The impact of the soil amendment on soil pH is clear, even at a few of the treated sites where there was subsequently little evidence for increased calcium or bicarbonate concentrations in the soil waters, as discussed below. It also noteworthy, in the context of results discussed below, that soils from sites BF6, BF2 and BF1 exhibited the highest post-amendment increases in pH value. Conversely, soils from sites BF3 and BF7 exhibited the smallest post-amendment shift in pH (Fig. 2).

#### 4.2.2. Weakly adsorbed (weak acid leachable) soil calcium

Leachable calcium refers to the Ca ion load that becomes adsorbed on clay mineral ion exchange sites and oxyhydroxide mineral surfaces in the soils following cation release by the weathering process. The leaching method used 10 mls 0.03M NaCl solution and 1g of soil as described by ten Berge et al. (2012). Duplicate leaching experiments were completed on two separate aliquots of the post-amendment soil samples collected on Oct. 16th 2021, approximately four months after the amendment was applied to the field. Duplicate leaching experiments were conducted on separate 1g and 2g aliquots of the archived October 2021 soils (Table S3; Fig. 3). The 2g leaching experiments were performed to achieve a more representative soil sample but solution/soil ratios were held constant in all experiments. Leachable calcium ranged from <10 mg Ca/kg soil for soils from the control sites to 175 mg Ca per kg soil for site BF1. While there is much scatter in the data, reflecting sample heterogeneity at the 1–2 g scale within the c. 1 kg soil samples, there is a statistically significant positive correlation ( $r^2 = 0.85$ ,  $p = 3.71E-7$ ) between loosely bound leachable calcium and post-amendment soil pH measured independently on the same soil aliquots (Fig. 3).

Excess leachable Ca, over and above that from the control sites, amounts to approximately  $19 \pm 7.5$  mg Ca/kg soil (Site BF7) up to  $161 \pm 20$  mg Ca/kg soil in the case of the soil from site BF1 (mean  $\pm$  1 standard deviation based on the duplicate leaches; Table S3). For reference, these amounts correspond to 1.1%–9.2% of the total calcium applied in the amendment, based on a nominal CRC amendment rate of 7.5 tonnes per ha, 43.41 wt % CaO (Table 2), a bulk soil density of 1.33 g/cm<sup>3</sup> and a mixing depth of 10 cm. This weathering and release of excess leachable calcium relative to the controls occurred over approximately 4 months (June 7th 2021 to October 16th) when the

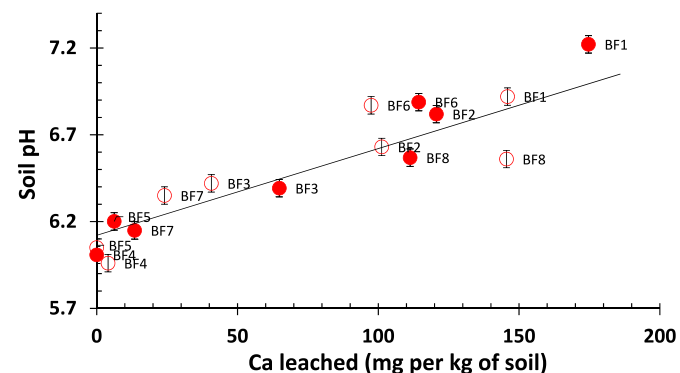


**Fig. 3.** Duplicate measurements of post-amendment soil pH vs. readily leachable calcium on soil samples taken on Oct 16th 2021. Leaching method used the protocol of ten Berge et al. (2012). Duplicate measurements were carried out on separate aliquots of soil from the same sample bag. Vertical error bars represent long-term typical 0.05 pH unit measurement reproducibility. Ca measurement uncertainties are <5% relative error ( $2\sigma$ ). A simple linear regression analysis (Pearson) confirms a statistically significant correlation ( $r^2 = 0.85$ ,  $p$  value < 0.001).

change in soil pH was most evident (Fig. 2). Soils from site BF8 show the second-highest weak-acid leachable calcium values ( $129 \pm 25$  mg Ca/kg soil). It is noticeable that soils from sites BF1 and BF8 that show the highest levels of weak-acid leachable Ca had the lowest soil pH values immediately after the amendment was applied (Fig. 2).

#### 4.2.3. Strong-acid soluble calcium

Soil calcium values from overnight strong acid (1M HNO<sub>3</sub>) leaching experiments of soils sampled in January 2022 are presented in Table S4 and Fig. S2. There is much heterogeneity and inter-site variability and no inferences about weathering rates can be drawn from the data. After 7 months, Ca values for soils at sites BF1 and BF6 remain significantly higher than inferred from the mean amendment rate (dashed line, Fig. S2) suggesting that these sites probably received higher than average amounts of CRC during the spreading operation. These sites also exhibit the highest soil pH (Fig. 2). For reference, the nominal soil amendment rate of 7.5 tonnes per ha would have added 2.33 tonnes Ca per ha, equivalent to approximately 1.75g Ca/kg soil, assuming a 10 cm mixing depth and a bulk soil density of 1.33 g/cm<sup>3</sup>.

#### 4.3. Soil water chemistry

Soil water chemistry data for the eight suction-cup samplers are given in Table 4. Soil water pH is generally in the range 6.6–7.4, with electrical conductivity in the range 160–600  $\mu$ S/cm and are generally classified as calcium-bicarbonate type waters on a Piper diagram (Fig. 4).

Total Alkalinity (TA) measurements by titration provide a measure of the total acid-neutralising capacity of a water and are based on titration of water sample to pH = 4.2. As discussed below, TA is dominated by bicarbonate ions in most of these waters. However, in some waters, other anions (e.g. nitrate, chloride, sulphate) could be relatively important, and for this reason we have also estimated bicarbonate concentrations using a charge-balance approach. Thus, the HCO<sub>3</sub><sup>−</sup> (mM) \* values shown in Table 4 were calculated independently using a charge balance method as [(Mg x 2) + (Ca x 2) + (K) + (Na) + (Fe x 2) + (Ba x 2) + (Sr x 2)] - [(F) + (Cl) + (Br) + (NO<sub>3</sub>) + ((SO<sub>4</sub>) x 2) + ((PO<sub>4</sub>) x 3)]. PHREEQC equilibrium thermodynamic modelling (Parkhurst and Appelo, 1999) confirmed that the HCO<sub>3</sub><sup>−</sup> ion accounts for 97–100% of the dissolved inorganic carbon species. The PHREEQC modelling also indicated that cation-hydrogen-bicarbonate complexes such as CaHCO<sub>3</sub><sup>+</sup> and MgHCO<sub>3</sub><sup>+</sup> which would not be captured by the alkalinity titration typically account for less than 1.5% ( $0.9 \pm 0.5\%$ ; average  $\pm 1\sigma$ ) of the

**Table 4**

Soil water geochemical data for soil waters from sites BF1 to BF8 collected on the dates shown. Designations n.m. and n.d. denote not measured (low sample volumes) and below detection limit respectively. All concentrations are in millimoles per litre except for Sr, Ba and Br which are in micromoles per litre. Tot. Alk is total alkalinity based on titration of water sample to pH = 4.2 and is expressed as mmol/L bicarbonate.  $\text{HCO}_3^-$  (mM)\* is calculated independently using a charge balance method as  $[(\text{Mg} \times 2) + (\text{Ca} \times 2) + (\text{K}) + (\text{Na}) + (\text{Fe} \times 2) + (\text{Ba} \times 2) + (\text{Sr} \times 2)] - [(\text{F}) + (\text{Cl}) + (\text{Br}) + (\text{NO}_3) + ((\text{SO}_4) \times 2) + ((\text{PO}_4) \times 3)]$ . PHREEQC speciation is shown in Table S5.

Site	Date	pH	Cond μS/cm)	Tot.Alk (mM $\text{HCO}_3^-$ )	$\text{HCO}_3^-$ (mM)*	Ca (mM)	Mg (mM)	K (mM)	Na (mM)	Sr (μM)	Ba (μM)	$\text{NO}_3$ (mM)	$\text{SO}_4$ (mM)	Cl (mM)	F (mM)	Br (μM)
BF1	16/ 07/21	6.71	182	1.58	1.41	0.49	0.18	0.03	0.43	0.35	1.51	0.09	0.05	0.15	0.01	n.d.
BF1	11/ 09/21	7.03	172	1.56	1.44	0.48	0.19	0.02	0.39	0.28	1.44	n.d.	0.07	0.17	0.01	n.d.
BF1	16/ 10/21	6.96	157	1.26	1.18	0.42	0.16	0.01	0.34	0.22	0.89	n.d.	0.05	0.21	0.02	2.13
BF1	23/ 11/21	6.63	173	1.26	1.22	0.45	0.18	n.m.	0.38	n.m.	n.m.	0.00	0.05	0.30	0.02	n.d.
BF1	24/ 12/21	6.74	174	1.21	1.04	0.42	0.19	0.02	0.38	0.23	1.01	0.03	0.05	0.42	0.02	2.70
BF1	01/ 04/22	n. m.	n.m.	1.50	1.35	0.48	0.22	0.02	0.41	0.23	n.m.	0.01	0.04	0.37	0.02	n.d.
BF2	16/ 07/21	7.08	437	3.74	3.21	1.09	0.43	0.20	0.99	1.07	1.48	0.12	0.15	0.58	0.02	3.08
BF2	09/ 08/21	6.85	312	2.96	1.86	0.39	0.32	0.14	0.77	0.36	1.31	0.02	0.10	0.22	0.03	n.d.
BF2	24/ 12/21	6.90	190	1.24	1.00	0.40	0.20	0.08	0.51	0.38	1.23	0.08	0.07	0.54	0.02	n.d.
BF2	01/ 04/22	n. m.	n.m.	1.60	1.14	0.43	0.22	0.07	0.37	0.33	0.42	0.03	0.07	0.41	0.02	n.d.
BF3	16/ 07/21	6.76	286	1.65	1.46	0.78	0.25	0.03	0.55	0.68	1.72	0.22	0.09	0.76	0.01	2.39
BF3	09/ 08/21	6.58	455	1.65	1.21	1.39	0.43	0.02	0.60	0.92	1.26	1.76	0.09	1.10	0.03	6.66
BF3	11/ 09/21	7.06	408	1.76	1.12	1.20	0.39	0.01	0.47	0.80	1.73	1.05	0.08	1.33	0.01	1.05
BF3	16/ 10/21	6.81	243	1.53	1.26	0.74	0.23	0.01	0.27	0.46	0.97	0.02	0.06	0.82	0.02	n.d.
BF3	23/ 11/21	6.71	215	1.35	1.29	0.63	0.20	n.m.	0.28	n.m.	n.m.	0.00	0.06	0.50	0.02	n.d.
BF3	24/ 12/21	6.76	197	1.36	1.05	0.57	0.20	0.01	0.27	0.43	1.19	0.04	0.07	0.57	0.02	n.d.
BF4	09/ 08/21	6.43	275	2.26	1.67	0.56	0.30	0.08	0.50	0.53	1.23	0.01	0.06	0.45	0.03	6.90
BF4	11/ 09/21	6.98	202	1.80	1.44	0.43	0.22	0.07	0.47	0.43	1.28	0.00	0.05	0.29	0.01	0.85
BF4	16/ 10/21	6.68	160	1.23	1.00	0.31	0.15	0.06	0.44	0.30	1.01	n.d.	0.05	0.32	0.02	n.d.
BF4	23/ 11/21	6.92	n.m.	n.m.	1.24	0.34	0.18	n.m.	0.63	n.m.	n.m.	0.01	0.04	0.32	0.02	n.d.
BF4	05/ 03/22	7.17	149	0.96	0.72	0.30	0.17	0.07	0.39	0.26	0.52	0.05	0.04	0.54	0.02	n.d.
BF5	16/ 07/21	6.72	205	1.64	1.54	0.48	0.26	0.05	0.50	0.47	1.71	0.08	0.10	0.17	0.02	2.23
BF5	09/ 08/21	6.42	174	1.62	1.54	0.44	0.25	0.03	0.43	0.32	1.09	n.d.	0.10	0.07	0.03	n.d.
BF5	11/ 09/21	6.98	166	1.53	1.41	0.40	0.23	0.03	0.39	0.30	1.05	n.d.	0.11	0.04	0.01	n.d.
BF5	16/ 10/21	6.69	136	1.14	1.01	0.30	0.17	0.02	0.35	0.20	0.81	0.00	0.12	0.06	0.02	n.d.
BF5	15/ 03/22	n. m.	n.m.	1.04	0.68	0.22	0.27	0.03	0.35	0.17	0.43	0.08	0.06	0.47	0.02	n.d.
BF5	01/ 04/22	6.77	179	2.00	1.19	0.45	0.28	0.03	0.35	0.28	0.46	0.01	0.06	0.50	0.02	3.27
BF6	16/ 07/21	7.00	473	4.43	4.06	1.36	0.67	0.07	0.69	1.05	1.56	0.01	0.12	0.48	0.02	3.85
BF6	09/ 08/21	6.75	522	5.60	5.24	1.69	0.90	0.06	0.54	1.00	1.01	n.d.	0.10	0.31	0.03	7.65
BF6	11/ 09/21	6.92	497	5.36	4.60	1.55	0.73	0.02	0.41	0.84	0.94	0.00	0.11	0.16	0.01	1.33
BF6	16/ 10/21	n. m.	n.m.	5.40	3.30	0.94	0.72	0.01	0.42	0.68	0.66	n.d.	0.11	0.22	0.00	n.d.
BF6	23/ 11/21	7.49	n.m.	6.22	5.75	1.72	0.95	n.m.	0.71	n.m.	n.m.	0.06	0.17	0.02	2.25	
BF6	22/ 01/22	7.32	655	7.21	7.03	2.12	1.46	0.02	0.60	1.15	1.08	0.00	0.05	0.62	0.02	4.96
BF6	15/ 03/22	n. m.	n.m.	7.44	7.12	2.26	1.42	0.02	0.52	1.12	0.37	0.00	0.05	0.66	0.02	5.27

(continued on next page)

**Table 4 (continued)**

Site	Date	pH	Cond μS/cm)	Tot.Alk (mM $\text{HCO}_3^-$ )	$\text{HCO}_3^-$ (mM)*	Ca (mM)	Mg (mM)	K (mM)	Na (mM)	Sr (μM)	Ba (μM)	$\text{NO}_3^-$ (mM)	$\text{SO}_4^-$ (mM)	Cl (mM)	F (mM)	Br (μM)
BF6	01/ 04/22	n. m.	n.m.	8.50	7.16	2.24	1.44	0.02	0.53	1.08	0.51	n.d.	0.04	0.65	0.02	4.87
BF7	16/ 07/21	7.31	486	3.76	3.62	1.62	0.45	0.09	0.76	1.14	1.40	0.17	0.29	0.61	0.02	3.35
BF7	11/ 09/21	7.35	364	3.53	2.97	1.17	0.34	0.04	0.50	0.75	0.92	0.01	0.20	0.14	0.01	n.d.
BF7	16/ 10/21	n. m.	n.m.	2.83	2.51	0.94	0.28	0.02	0.50	0.57	0.92	0.02	0.14	0.14	0.02	n.d.
BF7	24/ 12/21	7.36	241	2.05	1.85	0.70	0.27	0.02	0.55	0.51	1.69	0.06	0.14	0.30	0.02	n.d.
BF7	15/ 03/22	n. m.	n.m.	1.36	0.64	0.39	0.31	0.02	0.40	0.31	0.64	0.43	0.06	0.60	0.02	n.d.
BF8	16/ 07/21	6.93	595	5.31	4.06	1.76	0.45	0.13	0.76	1.52	1.27	0.01	0.26	0.69	0.02	3.84
BF8	09/ 08/21	6.67	456	4.36	1.81	0.58	0.35	0.07	0.70	0.59	1.03	n.d.	0.19	0.42	0.03	6.53
BF8	11/ 09/21	6.96	410	3.75	3.25	1.41	0.28	0.03	0.65	1.05	0.77	0.03	0.29	0.18	0.01	n.d.
BF8	16/ 10/21	6.86	398	2.76	2.19	1.24	0.23	0.03	0.67	0.86	0.66	0.49	0.32	0.32	0.02	n.d.
BF8	23/ 11/21	7.00	394	2.62	2.48	1.26	0.26	n.m.	0.84	n.m.	n.m.	0.38	0.36	0.29	0.02	n.d.
BF8	24/ 12/21	6.76	376	2.64	1.90	1.17	0.28	0.03	0.71	1.01	0.78	0.57	0.40	0.37	0.02	n.d.
BF8	22/ 01/22	8.86	344	2.28	2.35	1.14	0.31	0.04	0.74	1.02	0.73	0.46	0.25	0.36	0.02	n.d.
BF8	15/ 03/22	n. m.	n.m.	1.76	1.09	0.70	0.28	0.03	0.56	0.62	0.53	0.63	0.21	0.41	0.02	n.d.
BF8	01/ 04/22	7.01	388	2.88	2.04	1.02	0.26	0.03	0.50	0.84	0.45	0.14	0.21	0.48	0.02	n.d.

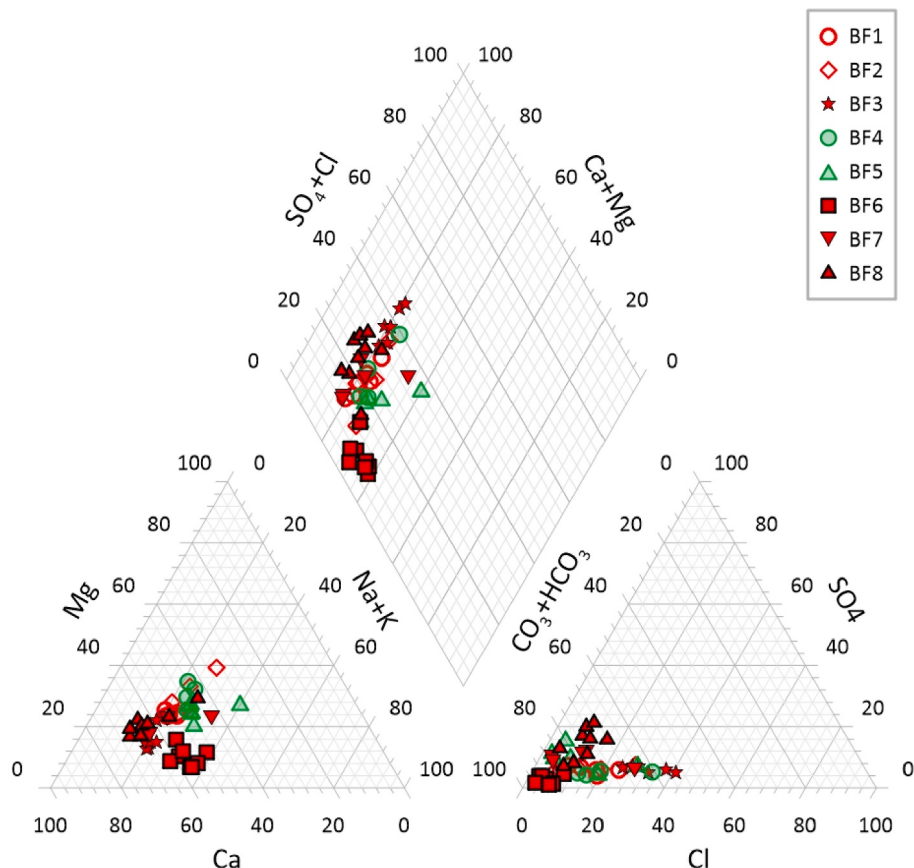


**Fig. 4.** Piper plot showing the Ca-bicarbonate nature of the soil-water samples. Note that samples plotted here were collected over the course of the study and there are some temporal trends in cations (e.g. Ca) and anions (e.g.  $\text{HCO}_3^-$ ) over time, although inter-site differences shown by the different symbol shapes are dominant. Green symbols denote control sites.

total DIC analysed by alkalinity titration. Similarly, these species ( $\text{CaHCO}_3^+$  and  $\text{MgHCO}_3^+$ ) generally account for less than 5% of the total Ca and Mg in the waters analysed by ICP (Table S5).

PHREEQC equilibrium thermodynamic geochemical modelling indicates that all soil waters apart from some BF6 samples, are undersaturated with respect to calcite and dolomite, using saturation indices for these minerals calculated for 10°C in PHREEQC (Table S5). No measurements of carbonate minerals in the soil were attempted, but pedogenic carbonate formation has never been reported in the region and is considered unlikely given the undersaturated state of most soil waters and the absence of pedogenic carbonates more widely in this relatively high rainfall region of NW Europe (Zamanian et al., 2016). High calcium and magnesium values (c. 2.3 and 1.5 mmol/L respectively) in the spring 2022 soil waters from the BF6 site result in saturation indices ( $\omega$ ) marginally higher than zero, indicating the potential for localised calcite precipitation, although kinetic inhibition of calcite precipitation is likely given the widespread occurrence of surface waters with calcite saturation indices  $>0$  (Knapp and Tipper, 2022). No carbonate was evident in the soil from simple acid dissolution tests although more sensitive test methods were not employed.

Considered as a group, soil-water bicarbonate values at the control sites (BF4 and BF5) are significantly lower than at the six other (amended) sites (mean bicarbonate alkalinity values of 1.43 vs. 3.14 mmol/L respectively), with a Welch two sample *t*-test  $p < 0.001$ . However, the bicarbonate concentrations as amended sites BF1, BF2 and BF3 are not statistically significantly different from the controls whereas those from sites BF6, BF7 and BF8 are all statistically different (higher) than the controls at the 95% confidence level.

Soil waters from the control sites have uniformly lower concentrations of calcium and total alkalinity compared with most of the sites in

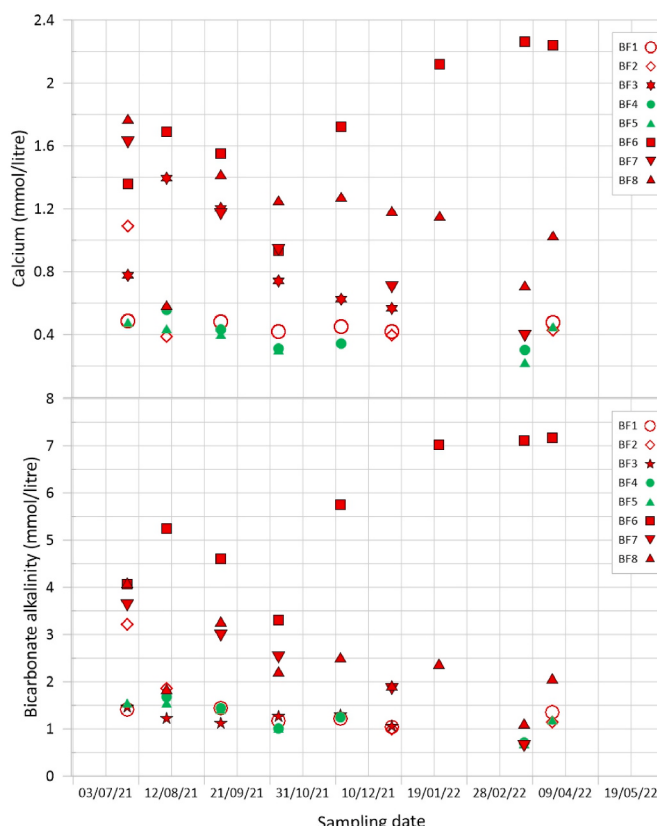


**Fig. 5.** Evolution of calcium and bicarbonate alkalinity (charge balance method as outlined in Table 4 caption) in soil waters at the eight sampling sites over the course of the study. Sites BF4 and BF5 (green symbols) are unamended control sites.

the amended sections of the field (Fig. 5).

Soil waters from two of the monitored sites (BF1 and BF2) close to the north-western edge of the field show only minimal increases in calcium relative to the controls (Fig. 5). Site BF3, in the north-west corner of the field and closest to the adjacent river shows increased calcium levels, but no increase in total alkalinity. Regardless of the calcium and bicarbonate results for the soil waters, it is worth recalling that all amended soils, including those sampled in the immediate vicinity of soil water samplers BF1, BF2 and BF3 show clear increases in soil pH (Fig. 2). As discussed below, waters from the BF3 site exhibit low bicarbonate/(Ca + Mg) molar ratios that may be linked to non-carbonic acid weathering. At most sites, both calcium and dissolved bicarbonate tend to decrease gradually with time over the course of the study (July 2021 to April 2022), apart from site BF6 which shows an increasing trend that appears to plateau near the end of the monitoring period. It is also noteworthy that the BF6 site showed the greatest initial increase in soil pH. Soils from the BF6 site also show highest strong-acid soluble calcium (Fig. S2).

Chloride, fluoride, sulphate and bromide anions in the soil waters show little evidence for systematic correlations or clear differences between sites or as a function of time, although average nitrate levels are highest in soil waters from sites BF3 and BF8. Soil waters from site BF8 and BF7 have highest sulphate levels (typically 0.1–0.4 mmol/L; Table 4) while highest chloride values occur in the BF3 soil waters (0.5–1.33 mmol/L; Table 4).

All soil waters are undersaturated with respect to gypsum, brucite, anhydrite, halite, and portlandite, but are supersaturated with respect to aluminium- and iron-bearing phases such as gibbsite and goethite. The latter is consistent with field observations of plough-disrupted ‘iron-pan’ fragments dispersed within the soil. Saturation indices with respect to a range of selected minerals, calculated using PHREEQC are shown in Table S5.

Molar ratios of bicarbonate to combined cations Ca and Mg cluster around the 2:1 line in Fig. 6 for most sites, consistent with weathering reactions that involve reactions between carbonic acid and hydroxides, silicates and carbonates. Weathering reactions driven by non-carbonic ‘strong’ acids (e.g. nitric) by contrast, would produce low bicarbonate to cation molar ratios. Samples from the BF3 and BF8 sites, unlike most other sites, are characterised by lower bicarbonate/(Ca + Mg) ratios in Fig. 6 and it is notable that the soil pH at these two sites never exceeded 6.6 (Fig. 2). Low soil-water bicarbonate/(Ca + Mg) ratios are generally associated with elevated concentrations of nitrate (Fig. 7).

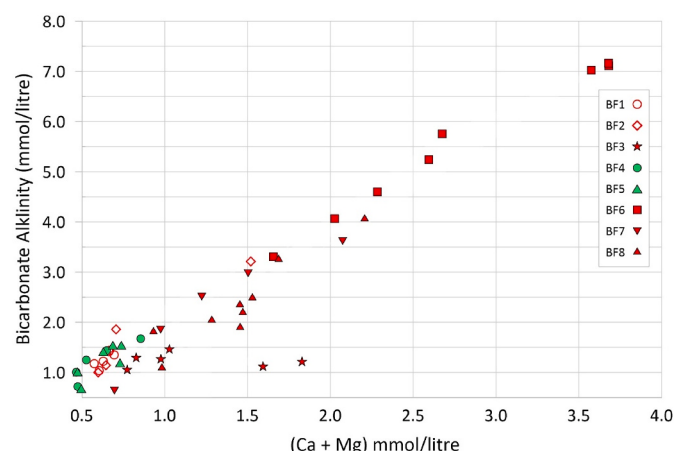


**Fig. 6.** Molar bicarbonate vs. molar concentrations of the major cations (Mg and Ca) in soil waters. Most of the data lie close to the 2:1 line as expected by bicarbonate-divalent cation charge balance, with the exception of most samples from sites BF3 and BF8.

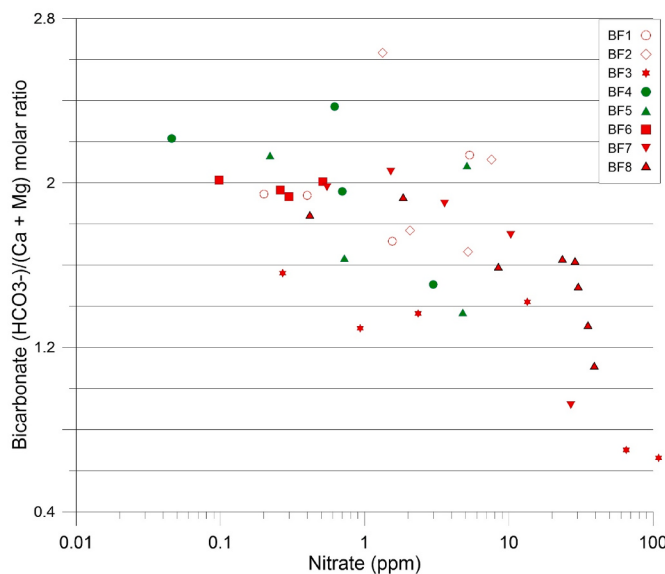


**Fig. 7.** Bicarbonate/(Ca + Mg) molar ratios are lowest in high nitrate samples.

## 5. Discussion

### 5.1. Potential CO<sub>2</sub> drawdown of CRC (R CO<sub>2</sub> values)

There is no generally accepted methodology to quantify CO<sub>2</sub> drawdown by enhanced weathering. Theoretical CO<sub>2</sub> drawdown values ( $RCO_2$ ; defined as the mass of CO<sub>2</sub> that could be captured per unit mass of weathered amendment) are often quoted in the literature to convey the relative CDR potential of different materials (Renforth and Henderson, 2017; Renforth, 2012, 2019; Lewis et al., 2021). This approach estimates maximum potential CO<sub>2</sub> drawdown based on the cation content of the amendment material and assuming that; (i) ultimately the amendment material weathers completely, releasing all its cations via drainage systems to the oceans and (ii) released cations are charge-balanced by bicarbonate generated as a result of carbonic-acid weathering and not by other anions such as nitrate, sulphate or chloride. In principle, bivalent cations such as Ca and Mg are twice as effective as monovalent cations and the method applies a correction for the likelihood that some of the weathering-released cations could be balanced by divalent carbonate ions (CO<sub>3</sub><sup>2-</sup>) as opposed to monovalent HCO<sub>3</sub><sup>-</sup> ions taking account of pH, pCO<sub>2</sub> and temperature-driven equilibria in the oceans (Renforth, 2019). Importantly, this stoichiometric approach takes no account of mineral dissolution kinetics which limits the fraction of an applied amendment that can be weathered within timescales that are both economic and relevant to climate mitigation. For context, typical RCO<sub>2</sub> values (mass ratios of maximum CO<sub>2</sub> removed per unit mass of amendment material) for basalts and similar mafic igneous rocks that are often considered as possible candidate soil amendments for CDR are typically in the range 0.30 ± 0.05, depending on their Mg and Ca contents. Calculated using similar methods (Renforth, 2019; Lewis et al., 2021), the CRC material has a relatively high RCO<sub>2</sub> value of 0.54, similar to the silicate mineral wollastonite (CaSiO<sub>3</sub>), reflecting its high calcium content (Table 2), but we have conservatively discounted this by 50% in Table 5 because, as discussed above, for CRC weathering, half of the balancing bicarbonate may be derived from geological carbon (limestone aggregate) on weathering (reaction 2).

Because of uncertainties surrounding possible non-carbonic acid weathering and how to correct for this, we have focused on bicarbonate measurements in the soil waters to derive our best estimates of CO<sub>2</sub> removal resulting from chemical weathering in this study.

**Table 5**

R values calculated for the CRC material using the method of Renforth (2019). Following Renforth (2019), a conservative  $\eta$  value of 1.5, reduced from a theoretical value of 2.0 is used to reflect the relative proportion of divalent carbonate to monovalent bicarbonate ions in ocean DIC at pH 8.2. For comparison R values have been calculated using the same methodology for other soil amendments. Basalts typically have R values of c. 0.3 depending on their composition. Pure wollastonite, a material that has been used for CDR by enhanced weathering (Haque et al., 2020) has a value of 0.58, although mined wollastonite for this purpose is likely to be relatively impure, with R values in the range 0.41–0.58. Major element ranges for wollastonite are from Deer et al. (2013).

	CRC material	Paleogene basalt (N. Ireland)	Wollastonite (CaSiO <sub>3</sub> )
CaO wt %	43.41 (Table 2)	10.55	34–48
MgO wt %	1.46 (Table 2)	7.58	0.26–0.85
Na <sub>2</sub> O wt %	0.10 (Table 2)	1.73	0–0.02
K <sub>2</sub> O wt %	0.40 (Table 2)	0.29	0–0.04
<i>R</i> value (tonne/tonne)	0.54 (reduced to 0.27)	0.27	0.41–0.58

### 5.2. Dissolution kinetics of CRC

A potential advantage of carbonate-rich soil amendments for CDR is their fast dissolution kinetics. A shrinking core dissolution model (Gbor and Jia, 2004; Renforth et al., 2015) was used to evaluate whether the observed rapid decline in soil water calcium contents (Fig. 5) accompanied by flattening of soil pH trends with time (Fig. 2) could reflect rapid weathering out of the CRC, albeit with significant retention of released Ca ions on the soil mineral ion-exchange sites. Calcite is the dominant calcium-bearing mineral phase of the material, accounting for 92% of its total calcium budget by mass based on the mineralogical and major element data (Tables 1 and 2). At the time of the XRD analysis (January 2022), portlandite accounted for only 2% of the calcium budget (0.8 wt% portlandite; Table 1), likely due to carbonation of the material during storage prior to analysis. For context, portlandite typically accounts for 25–30 wt % of fresh cement paste, depending on cement/water ratios (Aitcin, 2016). Depending on a concrete's cement to aggregate ratio, cement paste typically accounts for about a fifth by mass, implying that initial portlandite contents immediately after crushing is likely to be several wt %. This implies that substantial carbonation of the material must have occurred during post-crushing storage for >6 months between initial concrete crushing in June 2021 and the XRD analysis in January 2022 (Table 1). In a shrinking-core model to investigate changes in soil porewater calcium over time discussed below, we have conservatively used the low residual portlandite content of 0.8 wt%, as measured in January 2022. Based on equilibrium solubility data, portlandite is approximately 1500 times more soluble than calcite (Ruiz-Agudo et al., 2013), but data for its near-neutral pH steady state dissolution rate is constrained only by atomistic modelling (Izadifar et al., 2022), and varies by 16 orders of magnitude depending on the crystallographic faces undergoing dissolution. A mid-range rate of value of 10<sup>-6.6</sup> mol/m<sup>2</sup>/s was used but in practice, the choice of dissolution rate for portlandite has negligible effect on the outcome of the modelled calcium release from the CRC material, because of the overwhelming dominance of calcite. Aside from calcite and portlandite, the concrete contains almost 8 wt% amorphous material (Table 1) which is interpreted to reflect non-crystalline calcium silicate hydrate phases (CSH). These weakly-to non-stoichiometric phases arise in concrete from the hydration of di- and tri-calcium silicates within the cement paste fraction of the concrete and their experimentally determined steady-state dissolution rates range from 10<sup>-8</sup> to 10<sup>-11</sup> mol/m<sup>2</sup>/s depending on their Ca/Si ratios, assuming locally high mineral-adjacent pH values of 11–12.5 (Trapote-Barreira et al., 2014). Minor amounts of dolomite are also present, but its kinetics are relatively well constrained (Palandri and Kharaka, 2004).

The shrinking core model (reaction 8) is a simplification because it assumes spherical particles with initial diameter ( $D_0$ ).  $V_m$  is the molar volume of the mineral ( $\text{m}^3/\text{mol}$ ) and  $W_r$  is the mineral dissolution rate ( $\text{moles}/\text{m}^2/\text{s}$ ) for near neutral pH values after Palandri and Kharaka (2004). The model calculates  $X(t)$ , the fraction of the material dissolved as a function of time (s) using the standard simplified shrinking core equation:

$$X(t) = (D_0^3 - (D_0 - 2 * W_r * V_m * t)^3 / D_0^3) \quad (8)$$

For the purposes of the model, CRC with calcite:dolomite: CSH: portlandite in the proportions 85.35%, 0.2%, 9.6% and 0.0096% were used reflecting the normalised relative proportion of the main Ca-bearing phases in the XRD results (Table 1). In practice, varying the proportions of the minor constituents has little effect on the model output. Fig. 8 shows the results of a shrinking core model run based on the near-neutral pH dissolution rates of Palandri and Kharaka (2004). A mid-range portlandite dissolution rate of  $10^{-6.6} \text{ mol/m}^2/\text{s}$  (Izadifar et al., 2022) was used, along with the lower end of the range for CHS dissolution rates ( $10^{-11} \text{ mol/m}^2/\text{s}$ ). Whilst shrinking core models have their limitations, an important result is that a large fraction of the CRC material is predicted to weather within 12 months. The progressive decline in soil water calcium contents at most sites (Fig. 2) is consistent with rapid initial dissolution of the material followed by progressive flushing out of the calcium and bicarbonate from shallow soil levels over a c. 1 year timescale. The model also indicates that essentially all of the coarser (sub-4mm) size fraction dissolves in 1.5 years. Table 6 shows timescales for complete dissolution of CRC material as a function of particle diameters (see Fig. 9).

Soil waters from site BF6 are clearly exceptional because their Ca contents increase irregularly over the course of the study before reaching a plateau value for the last three months. It is noteworthy that the strong-acid soluble calcium (SASC) values for BF6 remain highest in the soils re-sampled in January 2022 (Fig. S2), suggesting that a higher amendment rate than average may have been applied to this part of the field during the spreading operation.

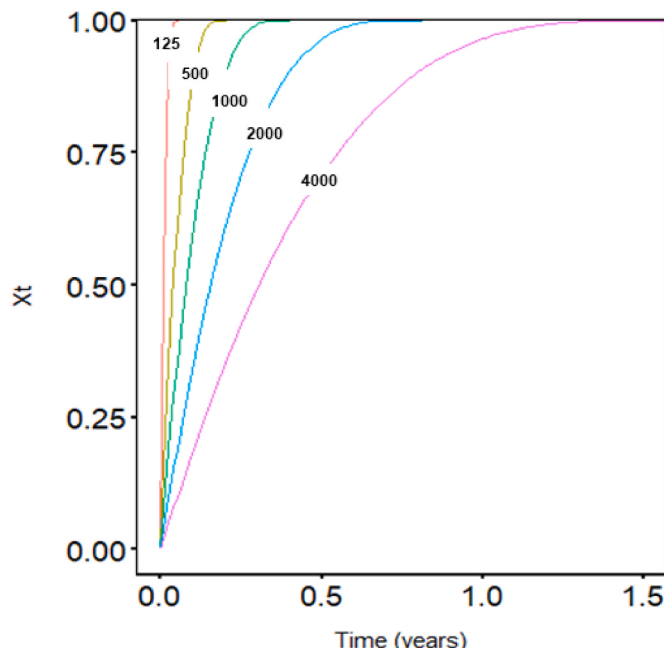


**Fig. 8.** Results from a shrinking core dissolution model for the CRC.  $X_t$  (y-axis) is the mass fraction of material dissolved as a function of time in years on x-axis. Left to right, the curves are for initial particle diameters of 125, 500, 1000, 2000 and 4000  $\mu\text{m}$ . Rapid dissolution of fines can explain the decline in soil water calcium values over the 10-month monitoring period at most sites (Fig. 5).

**Table 6**

Shrinking core model calculated times for complete dissolution of the modelled CRC mineralogy. Complete dissolution of even the coarsest fraction should be achieved after 1.5 years. After 10 months (June 2021–April 2022), only the relatively coarse fraction of the CRC should remain.

Spherical grain size (mm)	4	2	1	0.5	0.125
Dissolution time (y)	1.5	0.74	0.37	0.19	0.05

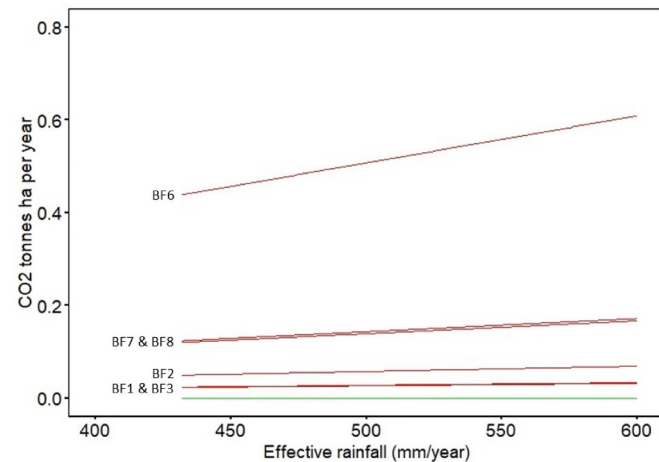


**Fig. 9.** Calculated  $\text{CO}_2$  drawdown (tonnes  $\text{CO}_2/\text{ha}$ ) based on modelled effective-rainfall and site-average bicarbonate concentrations in soil waters.

### 5.3. The calcium budget

A nominal amendment rate of 7.5 t/ha corresponds to 2.33 tonnes calcium/ha based on its major element composition (Table 2). Soil water calcium concentrations are variable, but typically show an initial increase of  $0.8 \pm 0.4 \text{ mmol/L}$  relative to controls (Fig. 5). Assuming an annual total downward water flux through the soil similar to the effective annual rainfall of  $514 \pm 86 \text{ mm}$ , the calculated annual soil-water calcium flux removed less than 10% of the total amount of calcium added by the amendment. As discussed above, fraction of calcium ions that were weakly adsorbed on negatively charged soil minerals and removed by the weak 0.03M NaCl leach (Fig. 3) after 4 months of weathering, could account for an additional 1.2–10.3% of the amendment-added calcium. In principle, uptake of calcium ions by crop plants could also account for some of the ‘missing’ calcium. Calcium, an essential plant nutrient can account for 0.1–4.4 dry weight % of plant tissue (White, 2001). The BF site was used to grow a mixed cereal/seed crop during the study period (barley, oats, linseed mix). Taking a typical low-input cereal production rate of 6–8 tonnes per hectare could account for up to 32 kg of calcium per ha or approximately 1% of the amendment-added calcium, assuming a typical calcium concentration of 0.2–4 g/kg for cereal grains (McKevith, 2004; Shobana et al., 2013). Taking other crop dry matter into account (e.g. straw residue) at a typical rate of up to 9 tonnes/ha and taking published calcium concentrations of up to 4000 ppm in wheat straw as an example (Le et al., 2014), would account for a further 36 kg Ca/ha. Additional calcium is likely to have been taken up by plant root biomass, but overall, it seems that a relatively small fraction of the added calcium (a few %) can have been taken up by plants at the BF site. An important question therefore is the fate of most of the amendment-supplied calcium. Calcium that is very strongly adsorbed on the surfaces of negatively charged soil particles would not be included in the dissolved fraction as measured by the soil pore-water chemistry (Fig. 5), nor would it have been removed by the relatively weak 0.03M NaCl leaching method. A more likely explanation is that a significant fraction of the weathering-released calcium

ions remains adsorbed on soil mineral surfaces by cation-exchange reactions. Hypothetically, a soil with a moderate cation exchange capacity of 10 meq/100g of soil for example could accommodate several tonnes of Ca per hectare if all available exchange sites were occupied by calcium ions, so in principle soil-adsorbed calcium could account for a major fraction of the total calcium budget.

Higher leachable calcium fraction in soils from amended sites compared with the controls are interpreted below to represent loosely bound calcium ions liberated by weathering of the amendment that remained weakly bound on negatively charged clay minerals and organic matter in the soil. The correlation between weakly adsorbed calcium (0.03M NaCl leach) and soil pH (Fig. 3) is consistent with cation exchange reactions on soil minerals involving  $\text{Ca}^{2+}$  and  $\text{H}^+$  ions.

Strong acid (1M) soluble calcium values for the soils sampled in January 2022 (Table S4) range from 2.15 to 8.69 mg/g soil, with values of c. 1.6–1.9 mg Ca/g soil at the control sites. After correction for the control site values it is clear that at most sites, the strong-acid soluble calcium had returned to values below the average value of 1.75 mg per kg soil that would be present if the applied 7.5 tonnes CRC per hectare was evenly distributed over the area of the field (Fig. S2). In the context of the soil-water calcium values (Fig. 5), it is noted that site BF6 shows the highest soil water Ca values, is close to saturation with respect to calcite and also shows the highest strong-acid soluble soil Ca (Fig. S2), whereas site BF1 exhibits low soil water Ca and dissolved bicarbonate, but high weak- and strong-acid soluble soil Ca. The latter may indicate strong cation adsorption at this high pH site (Figs. 2 and 3). The high strong-acid soluble calcium values at site BF6 are interpreted to reflect higher than average amendment application rates in this part of the field.

#### 5.4. The bicarbonate budget

Estimates of enhanced bicarbonate concentrations in soil waters (Table 7) were coupled with a simple soil-water infiltration model driven by effective annual precipitation described above to infer enhanced dissolved bicarbonate export rates from the soil. It is conservatively assumed that 50% of the enhanced bicarbonate observed in the soil waters results from soil gas  $\text{CO}_2$  although in practice any residual non-carbonated portlandite would have sequestered  $\text{CO}_2$  on a more favourable 1:1 M basis, and as discussed below, several % of the calcium carbonate in the CRC could have been produced by post-crushing atmospheric carbonation of portlandite (reaction 3). Time-weighted average bicarbonate concentrations in the soil waters, corrected for natural background weathering-produced bicarbonate using data from the two control sites are shown in Table 7. Also shown are estimated  $\text{CO}_2$  drawdown rates in units of tonnes  $\text{CO}_2 \text{ ha}^{-1} \text{ yr}^{-1}$  for meteoric water infiltration rates consistent with  $514 \pm 86 \text{ mm effective rainfall yr}^{-1}$  as discussed in the methods section above. CDR values in the range 27–520 kg  $\text{CO}_2$  per ha are estimated from these bicarbonate fluxes. Taking account of the amendment rate of 7.5 tonnes/ha, the 522 kg  $\text{CO}_2$  per ha per

year upper limit (Fig. 9) is about 4 times lower than implied by the maximum weathering potential calculation in Table 5. The highest (69 kg  $\text{CO}_2$  per tonne) estimate is for site BF6, but some of the soil waters at this site are close to chemical equilibrium with calcite (Table S1) which may constitute an upper limit for this material because calcite precipitation as a result of oversaturation of soil or drainage waters would precipitate carbonate and result in degassing and loss of the captured  $\text{CO}_2$  (reaction 5). The CDR values presented in Table 7 are conservative insofar as a 50% discount was applied to the enhanced soil-water bi-carbonate values, which may be pessimistic because some dissolve bi-carbonate could have been produced by dissolution of calcium carbonate after portlandite carbonation.

#### 5.5. Strong acid effects

A key requirement for successful CDR is that soil carbonic acid is the weathering agent, and that weathering by co-existing strong acids in soils (e.g. nitric or sulphuric acid; Spence and Telmer, 2005; Andrews and Taylor, 2019) is minimal. Elimination of strong acid effects or careful selection of sites is critical for amendments such as the CRC that contain carbonates because of the risk of  $\text{CO}_2$  production. Strong acids can arise in intensively fertilised soils where acidification results from nitrification of ammonium. In principle, amendments that contain significant quantities of ferrous iron (e.g. basalts) could also generate strong-acids by oxidation of ferrous iron-bearing minerals (Drever, 1997) in oxic soils. Soil waters from some sites, notably BF3 and to a lesser extent BF8, exhibit low bicarbonate/(Ca + Mg) molar ratios (Fig. 6), indicating non-carbonic acid weathering effects locally, probably driven by proton-generating nitrification reactions, given the tendency for high nitrate concentrations in these waters that have low bicarbonate/(Ca + Mg) ratios.

The extent to which  $\text{CO}_2$  generation could have occurred at the strong acid affected sites is not known because soil-gas flux measurements were outside the scope of the study. A simple stoichiometric  $\text{CO}_2$  production model in which half a mole of  $\text{CO}_2$  is produced per mole of nitrate released to the water (reaction 6) is used to estimate the magnitude of this effect and to assess the overall balance between  $\text{CO}_2$  production at strong-acid dominated sites vs.  $\text{CO}_2$  sequestration as dissolved bicarbonate. Results are shown in Fig. 10 for an example of 514 mm/year effective rainfall and average nitrate measured concentrations in the soil waters at each site. Blue bars reflect the raw  $\text{CO}_2$  drawdown rates depicted in Fig. 10, red bars show  $\text{CO}_2$  production predicted using the 0.5:1  $\text{CO}_2$ : nitrate (reaction 6) and green bars show the resulting balance. Importantly, even at the high nitrate site (BF3) the  $\text{CO}_2$  balance is essentially neutral and at all other sites there is net  $\text{CO}_2$  drawdown (conversion to bicarbonate), up to 0.52 tonnes  $\text{CO}_2/\text{ha}$  at site BF6. The model is an oversimplification insofar as it assumes that all nitrate is produced by nitric acid generated via the nitrification of ammonium, which results in an overall 0.5:1  $\text{CO}_2$ :nitrate molar stoichiometry. Fertilisers containing calcium nitrate could also produce nitrate without

**Table 7**

Table shows time-weighted milli-molar concentrations of bicarbonate (control corrected). The right-hand column shows calculated  $\text{CO}_2$  drawdown rates (tonnes  $\text{CO}_2$  per ha), based on effective rainfall (rainfall minus potential evapotranspiration) ( $\text{mm yr}^{-1}$ ) calculated from meteorological data ( $\pm 1$  standard deviation). A background bicarbonate value of 1.0 mmol/L (average of values from the control sites BF4 & BF5) has been subtracted from the raw measured values to calculate  $\Delta \text{HCO}_3^-$ . Uncertainties in column three reflect uncertainties in effective annual rainfall (soil water fluxes) only.

Soil water sample site	Time-weighted $\text{HCO}_3^-$ concentration (mmol/litre)	Control-corrected $\text{HCO}_3^-$ concentration (mmol/litre) referred to as $\Delta \text{HCO}_3^-$	$\text{CO}_2$ tonnes sequestered per hectare based on time-weighted $\Delta \text{HCO}_3^-$ and $514 \pm 86 \text{ mm effective rainfall yr}^{-1}$ and 50% discount as discussed in the text
BF1	1.24	0.24	$0.027 \pm 0.004$
BF2	1.52	0.52	$0.059 \pm 0.010$
BF3	1.25	0.25	$0.028 \pm 0.005$
BF4 (control)	0.81	–	–
BF5 (control)	1.21	–	–
BF6	5.61	4.61	$0.522 \pm 0.091$
BF7	2.30	1.30	$0.147 \pm 0.026$
BF8	2.26	1.26	$0.143 \pm 0.025$

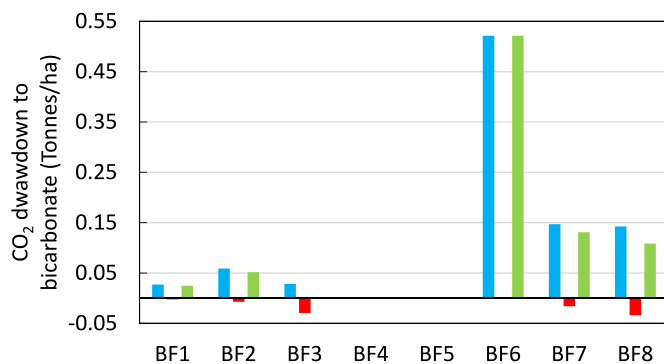


**Fig. 10.** Bars show gross (blue) and net (green) CO<sub>2</sub> drawdown in units of tonnes per hectare. Red bars denote negative drawdown (i.e. CO<sub>2</sub>) production and account for the difference between gross and net figures. At site BF3, the site most impacted by strong-acid weathering, the balance is approximately zero, but net CO<sub>2</sub> drawdown occurred at the five other amended sites. Taking account of the emissions associated with crushing, loading and transport (Table S9), half of the sites (BF6, BF7, BF8) achieved net CO<sub>2</sub> drawdown (BF2 is marginal).

nitrification, acidification and CO<sub>2</sub> production. Similarly, nitrate production by weathering carbon-free minerals such as portlandite (e.g. reaction 8) is ignored with the result that the calculated CO<sub>2</sub> production values may be over-estimated.

### 5.6. Other risks and uncertainties

While enhanced weathering is a promising approach for large-scale CDR, many uncertainties remain. These uncertainties include the possible short- and long-term unintended ecological and geochemical impacts on agricultural soils, surface and groundwaters. There are also uncertainties about how any resulting changes in soil pH might impact the cycling of nitrogenous compounds in soils including N<sub>2</sub>O production, with divergent effects reported for soils and their adjacent surface drainage systems (Kantola et al., 2017; Rosi-Marshall et al., 2016). Additionally, there is ongoing uncertainty about the possible impact of rapid soil pH adjustments on the stability of soil organic carbon (SOC) pools (Grover et al., 2021) and any loss of CO<sub>2</sub> through enhanced SOC turnover would not be detected in the absence of comprehensive soil-gas flux measurements in the days to months after amendment application.

Based on our analyses of the CRC material, no concerns arise from a metal contamination perspective, although batches of CRC would have to be analysed on an ongoing basis to ensure that concentrations are within acceptable (e.g. lime regulation) limits. The material could provide trace amounts of Cu and Zn in some metal-deficient soils, although it should be noted that excessive applications could result in elevated soil pH values which could lead to reduced trace metal bioavailability for crops in some soils.

An important consideration for future work is that combinations of dissolved bicarbonate, calcium concentrations and water pH that could result in over-saturation of soil waters by carbonate minerals such as calcite must be avoided, because re-precipitation of carbonates would result in complete loss of any sequestered CO<sub>2</sub> (reaction 5). Site BF6 provides an example of a soil water that is at or close to saturation with respect to carbonate minerals (Table S5), suggesting that a ΔHCO<sub>3</sub> value of approximately 6 mM/L may be a practical upper limit for this high-Ca alkaline material at typical near-neutral pH values. More broadly, global river water geochemical data support this upper estimate. For example, in the GLORICH database (Hartmann, 2014; Hartmann et al., 2019), a comprehensive global compilation of more than 1.27 million river water samples from >17,000 sampling locations worldwide, bicarbonate concentrations rarely exceed 5–6 mM/L. Taking a relatively favourable case in which ΔHCO<sub>3</sub> is approximately 5 mM/L implies that CO<sub>2</sub> drawdown would be limited to approximately 0.55 tonnes CO<sub>2</sub> per ha

for an effective rainfall (annual soil-water throughput) of 500 mm/year, limited by bicarbonate export rates. Although more data are required, the present indications are that the CRC material weathers quickly, and re-application at low annual rates of a few tonnes per hectare for several years depending on soil pH response, may be a useful strategy to avoid oversaturation of soil waters with respect to carbonates and consequent CO<sub>2</sub> loss.

Once exported to surface drainage, a remaining question is the extent to which the carbonate equilibria could shift away from bicarbonate dominance towards dissolved CO<sub>2</sub> if low pH streams and rivers are encountered. Many surface waters are supersaturated with respect to CO<sub>2</sub> resulting in CO<sub>2</sub> degassing (Butman and Raymond, 2011; Horgby et al., 2019), but the sources of CO<sub>2</sub> are highly variable in time and space. Of relevance to the current discussion is the fraction of the degassed CO<sub>2</sub> that has resulted from the EW-driven conversion of CO<sub>2</sub> to bicarbonate, and not the other baseline sources of riverine dissolved CO<sub>2</sub> such as plant respiration. Importantly, higher alkalinity levels in freshwaters that would result from carbonic-acid driven weathering of soil amendments such as CRC would lower existing levels of natural CO<sub>2</sub> degassing, particularly in low order streams (Stets et al., 2017), arguably representing an additional sink for CO<sub>2</sub> that would not be present in the absence of EW-driven enhanced riverine pH. Taking dissolved inorganic carbon (DIC) speciation into account, recipient drainage systems should probably have pH values in the range 7–8 to retain the bulk of the DIC as bicarbonate to avoid evasion of CO<sub>2</sub> at low pH, and carbonate precipitation in high pH systems. Similarly, caution would be required if receiving surface waters had been acidified, for example by acid rain or by coniferous afforestation upstream in a catchment. Acidic river catchments could convert bicarbonate to carbonic acid, leading to CO<sub>2</sub> evasion to the atmosphere.

The CDR potential offered by direct portlandite and calcium silicate hydrate (C-S-H) carbonation of the CRC material during storage under humid outdoor atmospheric conditions at the post-crushing, pre-amendment stage could also be optimised. Portlandite (Ca(OH)<sub>2</sub>), carbonation consumes 1 mol of CO<sub>2</sub> per mole of mineral carbonated (reaction 3). Taking the simple equimolar Ca(OH)<sub>2</sub>:CaCO<sub>3</sub> stoichiometry of reaction 3, an initial portlandite content of 4% by mass in the freshly crushed concrete, (derived by assuming 20% by mass initial portlandite in the cement paste (von Greve-Dierfeld et al., 2020) and a 5:1 aggregate:cement mass ratio), indicates a potential direct uptake of approximately 0.024 tonnes of CO<sub>2</sub> per tonne of concrete via portlandite carbonation. Taking account of the additional carbonation potential of the calcium silicate hydrate (C-S-H) phases in concrete indicates that 0.4–0.5 tonnes CO<sub>2</sub> can be bound per tonne of ordinary portlandite cement (OPC), (von Greve-Dierfeld et al., 2020). This in turn suggests a total carbonation potential of c. 0.08–0.1 tonnes CO<sub>2</sub> per tonne of concrete that initially contained 20% OPC by mass. In practice these estimates are likely to be limited by reaction kinetics, and discounts would also have to be applied for the counter-factual (i.e. carbonation which would have occurred slowly, on decadal to centennial timescales within roughly broken or crushed stockpiles of returned concrete, in the absence of additional crushing to <4 mm grain size for the purposes of producing the soil amendment CRC). Future studies might consider using carbon isotopes to track the fraction of atmospheric carbon fixed by post-crushing sub-aerial carbonation before the material is applied as a soil amendment.

Several factors indicate that from an operational perspective, the energy and carbon penalty of utilising CRC as a soil amendment for CDR is likely to be lower than for alternative materials (e.g. olivine or basalt) which are quarried and crushed specifically for CDR purposes. First, the energy requirement to crush limestone-rich concrete is likely to be lower than for unaltered mafic rocks which typically have high specific crushing energy values (e.g. Korman et al., 2015) and require comminution to smaller grain sizes (<100 µm) to achieve dissolution on timescales of a few years (Renforth, 2012). Second, the distributed nature of concrete production facilities globally and relative proximity to

farms implies that post-crushing transport distances of bulk material, an important contributor to the overall energy and carbon footprints of enhanced weathering operations (Hartmann et al., 2013), are likely to be lower compared with less widely distributed mafic rocks and minerals. Details of a preliminary life cycle analysis (LCA), including crushing and transport-related emissions based on measurements and estimates from the literature (Renforth, 2012; Lefebvre et al., 2019; Moosdorff et al., 2014; Musci et al., 2019) are presented in Table S9, and detailed calculations are provided in Supplementary Excel® file 1. This simplified LCA indicates combined CO<sub>2</sub> emissions from crushing, loading, road transport and on-farm spreading of approximately 7.32 kg CO<sub>2</sub> per tonne of CRC, or approximately 11% of the c. 69 kg CO<sub>2</sub>/tonne inferred for the ‘best performing’ BF6 field site (Fig. 10). Taking these operations-related CO<sub>2</sub> emissions into account, strong-acid corrected CO<sub>2</sub> drawdown at sites BF1 and BF3 site are too low to offset operation-related emissions, site BF2 is marginal, but net CO<sub>2</sub> drawdown was achieved at three of the six field sites (BF6, BF7, BF8).

CRC availability is estimated to be in the order of 250–1000 Mt annually (1–4% of 25 Gt global concrete production; Ren et al., 2022; Xuan et al., 2016). Optimally, where CDR deployment is tuned to approach the theoretical potential of the material (Table 5), CDR rates in the order 68 to 270 Mt CO<sub>2</sub> annually could be achieved, a useful contribution to global CDR efforts towards Gt/year quantities (Beerling et al., 2020). Geochemical insights gained by its deployment could also pave the way for CDR strategies that involve better practices of deployments of agricultural ground limestone, a material that is currently considered (IPCC et al., 2021) to be a CO<sub>2</sub> source, regardless of soil conditions.

## 6. Conclusions

Weathering of carbonate-rich crushed returned concrete occurred rapidly within the first year after application to a tillage field in SE Ireland, consistent with the rapid dissolution rates inferred from a simple shrinking-core model. Soil water samples for most amended sites show clear evidence for elevated calcium and bicarbonate concentrations relative to the control sites, and most soil waters exhibit high bicarbonate to calcium molar ratios expected from a carbonate-dominated system with minor residual calcium hydroxides. Two sites (BF3, and to a lesser extent BF8) that have high soil water nitrate concentrations and show evidence for non-carbonic dominated weathering, resulting in low bicarbonate to cation ratios. A challenge for future deployment of enhanced weathering at scale will be the development of cost-effective methods to detect and avoid non-carbonic acid ‘hotspots’ in fields and to assess their impact on overall CO<sub>2</sub> budgets. The latter is particularly a concern for carbonate-rich amendments such as the CRC material used here, but it also potentially a concern for high application-rate deployments of crushed basalt for CDR if minor amounts of secondary carbonates are present (e.g. Kemp et al., 2022).

Strong spatial heterogeneities in soil-water bicarbonate concentrations pose a challenge for efforts to scale-up enhanced weathering as a CDR technology. Further work is required to investigate whether intermediate-scale drainage systems (e.g. field tile drains) could be used to better integrate spatially variable bicarbonate ion production, although the potential for these systems to degas CO<sub>2</sub> when drainage water emerges from soils also requires consideration. Finally, in this study, a large fraction of the weathering-released calcium and magnesium cations apparently remain bound to exchange sites in the soil, and gradual release of these cations over time could allow further conversion of dissolved CO<sub>2</sub> to bicarbonate ions in the soil waters, but bicarbonate export rates by rivers may ultimately be the rate-limiting step.

## CRediT authorship contribution statement

**Frank McDermott:** Writing – review & editing, Writing – original draft, Visualization, Validation, Supervision, Software, Resources,

Project administration, Methodology, Investigation, Funding acquisition, Formal analysis, Data curation, Conceptualization. **Maurice Bryson:** Writing – review & editing, Resources, Project administration, Investigation, Funding acquisition, Conceptualization. **Ruadhan Magee:** Writing – review & editing, Methodology. **David van Acken:** Writing – review & editing, Software, Resources, Methodology, Investigation.

## Declaration of competing interest

The authors declare the following financial interests/personal relationships which may be considered as potential competing interests:

Maurice Bryson reports a relationship with Silicate Ltd that includes: equity or stocks. Other authors declare that they have no known competing financial interests or personal relationships that could have appeared to influence the work reported in this paper.

## Data availability

Data will be made available on request.

## Acknowledgements

The authors acknowledge support from an Enterprise Ireland Innovation Voucher for partially funding the initial stages of this work. This publication has emanated from research conducted with the financial support of Science Foundation Ireland under Grant number 13/RC/2092\_P2. For the purpose of Open Access, the author has applied a CC BY public copyright licence to any Author Accepted Manuscript version arising from this submission. M.B. and FMcD thank landowners Denis and Jane O’Connell for their kind hospitality and for allowing access to their farm during fieldwork for the project.

## Appendix A. Supplementary data

Supplementary data to this article can be found online at <https://doi.org/10.1016/j.apgeochem.2024.106056>.

## References

- Aïtcin, P.-C., 2016. Portlandite cement. In: Aïtcin, P.-C., Flatt, R.J. (Eds.), *Science and Technology of Concrete Admixtures*. Elsevier, pp. 27–51 (Chapter 3).
- Andrews, M.G., Taylor, L.L., 2019. Combating climate change through enhanced weathering of agricultural soils. Elements 15, 253–258. <https://doi.org/10.2138/gselements.15.4.253>.
- Arevalo Jr., R., McDonough, W.F., 2010. Chemical variations and regional diversity observed in MORB. Chem. Geol. 271, 70–85.
- Baek, S.H., Kanzaki, Y., Lora, J.M., Planavsky, N., Reinhard, C.T., Zhang, S., 2023. Impact of climate on the global capacity for enhanced rock weathering on croplands. Earth's Future 11, e2023EF003698.
- Barnes, S.J., Zhou-Sen, Y., Mao, Y.J., et al., 2023. Nickel in olivine as an exploration indicator for magmatic Ni-Cu sulfide deposits: a data review and re-evaluation. Amer. Mineral. 108, 1–17.
- Beerling, D.J., Kantzias, E.P., Lomas, M.R., Wade, P., Eufrasio, R.M., Renforth, P., Sarkar, B., Andrews, M.G., James, R.H., Pearce, C.R., Mercure, J.F., Pollitt, H., Holden, P.B., Edwards, N.R., Khanna, M., Koh, L., Quegan, S., Pidgeon, N.F., Janssens, I.A., Hansen, J., Banwart, S.A., 2020. Potential for large scale CO<sub>2</sub> removal via enhanced weathering with croplands. Nature 583, 242–248.
- Berner, E.K., Berner, R.A., 1987. *The Global Water Cycle: Geochemistry and Environment*. Prentice-Hall.
- Brunauer, S., Emmett, P.H., Teller, E., 1938. Adsorption of gases in multimolecular layers. J. Am. Chem. Soc. 60, 309–319.
- Buckingham, F.L., Henderson, G.M., Holdship, P., Renforth, P., 2022. Soil core study indicates limited CO<sub>2</sub> removal by enhanced weathering in dry croplands in the UK. Appl. Geochem. 147, 105482.
- Butman, D., Raymond, P.A., 2011. Significant efflux of carbon dioxide from streams and rivers in the United States. Nat. Geosci. 4 (12), 839–842.
- Cerling, T.E., 1984. The stable isotopic composition of modern soil carbonate and its relationship to climate. Earth Planet. Sci. Letts. 71, 229–240.
- Coufalik, P., Krmicek, L., et al., 2018. Model of mercury flux associated with volcanic activity. Bull. Env. Cont. and Toxicol. 101, 549–553.
- Deer, W.A., Howie, R.A., Zussman, J., 2013. *An Introduction to the Rock-Forming Minerals*, third ed. cm. ISBN ISBN 978-0903056-33-5.

- Dietzen, C., Rosing, M.T., 2023. Quantification of CO<sub>2</sub> uptake by enhanced weathering of silicate minerals applied to acidic soils. *Int. J. Greenh. Gas Control* 125, 103872.
- Drever, J.I., 1997. The Geochemistry of Natural Waters: Surface and Groundwater Environments, third ed. Prentice Hall, New Jersey.
- Estokova, A., Palascakova, L., Kanuchova, M., 2018. Study on Cr(VI) leaching from cement and cement composites. *Int. J. Environ. Res. Public Health* 15, 824. <https://doi.org/10.3390/ijerph15040824>, 2018.
- EU, 2019. Regulation (EU) 2019/1009 of the European Parliament and of the Council Laying Down Rules on the Making Available on the Market of EU Fertilizing Products and Amending Regulations (EC) No 1069/2009 and (EC) No 1107/2009 and Repealing Regulations (EC) No 2003/2003.
- Flipkins, G., Blust, R., Town, R.M., 2021. Deriving nickel (Ni(II)) and chromium (Cr(III)) based environmentally safe olivine guidelines for coastal enhanced silicate weathering. *Environ. Sci. Technol.* 55, 12362–12371.
- Fuss, S., Canadell, J., Peters, G., et al., 2014. Betting on negative emissions. *Nature Clim Change* 4, 850–853.
- Gabe, U., Rodella, A.A., 1999. Trace elements in Brazilian agricultural limestones and mineral fertilizers. *Commun. Soil Sci. Plant Anal.* 30 (5 & 6), 605–620.
- Gale, A., Dalton, C.A., Langmuir, C.H., Su, Y., Schilling, J.-G., 2013. The mean composition of ocean ridge basalts. *Geochim. Geophys. Geosyst.* 14, 489–518. <https://doi.org/10.1029/2012GC004334>.
- Gardiner, M.J., Ryan, P., 1969. A New Generalised soil Map of Ireland and its land-use interpretation. *Irish J. Ag. Res.* 8 (1), 95–109. <https://www.jstor.org/stable/2555514>.
- Gastmans, D., Hutcheon, I., Antônio Menegário, A., Chang, H.K., 2016. Geochemical evolution of groundwater in a basaltic aquifer based on chemical and stable isotopic data: case study from the Northeastern portion of Serra Geral Aquifer, São Paulo state (Brazil). *J. Hydrol.* 535, 598–611. <https://doi.org/10.1080/00103629909370231>.
- Gbor, P.K., Jia, C.Q., 2004. Critical evaluation of coupling particle size distribution with the shrinking core model. *Chem. Eng. Sci.* 59, 1979–1987.
- Goll, D.S., Ciais, P., Amann, T., Buermann, W., Chang, J., Eker, S., et al., 2021. Potential CO<sub>2</sub> removal from enhanced weathering by ecosystem responses to powdered rock. *Nat. Geosci.* 14, 545–549. <https://doi.org/10.1038/s41561-021-00798-x>.
- Grover, S.P., Clayton, R.B., Wang, X., Gleeson, D.B., Macdonald, L.M., Tang, C., 2021. Liming and priming: the long-term impact of pH amelioration on mineralisation may negate carbon sequestration gains. *Soil Security* 3, 100007.
- Haque, F., Chiang, Y.W., Santos, R.M., 2019. Alkaline mineral soil amendment: a climate change ‘stabilization wedge’. *Energies* 12, 2299. <https://doi.org/10.3390/en12122299>.
- Haque, F., Santos, R.M., Chiang, Y.W., 2020. CO<sub>2</sub> sequestration by wollastonite-amended agricultural soils – an Ontario field study. *Int. J. Greenhouse Gas Cont.*, 103017.
- Hartmann, J., et al., 2014. A Brief Overview of the GLObal RIver Chemistry Database. GLORICH. *Procedia Earth and Planetary Science* 10, 23–27. <https://doi.org/10.1016/j.proeps.2014.08.005>.
- Hartmann, J., Lauerwald, R., Moosdorff, N., 2019. GLORICH - Global river chemistry database [dataset]. <https://doi.org/10.1594/PANGAEA.902360>.
- Hartmann, J., West, A.J., Renforth, P., Köhler, P., De La Rocha, C.L., Wolf-Gladrow, D.A., Dürr, H.H., Scheffran, J., 2013. Enhanced chemical weathering as a geoengineering strategy to reduce atmospheric carbon dioxide, supply nutrients, and mitigate ocean acidification. *Rev. Geophys.* 51, 113–149. <https://doi.org/10.1002/rog.20004>.
- Horgby, A., Segatto, P.L., Bertuzzo, E., Lauerwald, R., Lehner, B., Ulseth, A.J., Vennemann, T.W., Battin, T., 2019. Unexpected large evasion fluxes of carbon dioxide from turbulent streams draining the world’s mountains. *Nat. Comm.* 10, 4888. <https://doi.org/10.1038/s41467-019-12905-z>.
- Hughes, A.L.C., Gyllencreutz, R., Lohne, Ø.S., Mangerud, J., Svendsen, J.I., 2016. The last Eurasian ice sheets – a chronological database and time-slice reconstruction, DATED-1. *Boreas* 45, 1–45. <https://doi.org/10.1111/bor.12142> ISSN 0300-9483.
- IPCC, 2021. In: Masson-Delmotte, V.P., Zhai, A., Pirani, S.L., Connors, C., Péan, S., Berger, N., Caud, Y., Chen, L., Goldfarb, M.I., Gomis, M., Huang, K., Leitzell, E., Lonnoy, J.B.R., Matthews, T.K., Maycock, T., Waterfield, O., Yu, Yelekçi R., Zhou, B. (Eds.), Climate Change 2021: the Physical Science Basis: Contribution of Working Group I to the Sixth Assessment Report of the Intergovernmental Panel on Climate Change. Cambridge University Press.
- Izadifar, M., Ukrainczyk, N., Salah Uddin, K.M., Middendorf, B., Koenders, E., 2022. Dissolution of portlandite in PureWater: Part 2 atomistic kinetic Monte Carlo (KMC) approach. *Materials* 15, 1442. <https://doi.org/10.3390/ma15041442>.
- Kantola, I.B., Masters, M.D., Beerling, D.J., Long, S.P., DeLucia, E.H., 2017. Potential of global croplands and bioenergy crops for climate change mitigation through deployment for enhanced weathering. *Biol. Lett.* 13, 20160714 <https://doi.org/10.1098/rsbl.2016.0714>.
- Kantola, I.B., Blanc-Betés, E., Masters, M.D., et al., 2023. Improved net carbon budgets in the US Midwest through direct measured impacts of enhanced weathering. *Glob. Change Biol.* 2023, 1–17. <https://doi.org/10.1111/gcb.16903>, 00.
- Kantz, E.P., et al., 2022. Substantial carbon drawdown potential from enhanced rock weathering in the United Kingdom. *Nat. Geosci.* 15, 382–389.
- Kelland, M.E., Wade, P.W., Lewis, A.L., et al., 2020. Increased yield and CO<sub>2</sub> sequestration potential with the C4 cereal Sorghum bicolor cultivated in basaltic rock dust-amended agricultural soil. *Glob. Change Biol.* 26, 3658–3676.
- Kemp, S.J., Lewis, A.L., Rushton, J.C., 2022. Detection and quantification of low levels of carbonate mineral species using thermogravimetric-mass spectrometry to validate CO<sub>2</sub> drawdown via enhanced rock weathering. *Appl. Geochem.* 146, 105465.
- Keppert, M., Davidová, V., Doušová, B., Scheinherrová, L., Reiterman, P., 2021. Recycling of fresh concrete slurry waste as supplementary cementing material: characterisation, application and leaching of selected elements. *Construct. Build. Mater.* 300, 124061.
- Knapp, W.J., Tipper, E.T., 2022. The efficacy of enhancing carbonate weathering for carbon dioxide sequestration. *Front. Clim.* 4, 928215 <https://doi.org/10.3389/fclim.2022.928215>.
- Korman, T., Bedekovic, G., Kujundzic, T., Huhinek, D., 2015. Impact of physical and mechanical properties of rocks on energy consumption of jaw crusher. *Physicochem. Probl. Miner. Process.* 51 (2), 461–475.
- Larkin, C.S., Andrews, M.G., Pearce, C.R., Yeong, K.L., Beerling, D.J., Bellamy, J., Benedick, S., Freckleton, R.P., Goring-Harfard, H., Sadekar, S., James, R.H., 2022. Quantification of CO<sub>2</sub> removal in a large-scale enhanced weathering field trial on an oil palm plantation in Sabah, Malaysia. *Front. Clim.* 4, 959229 <https://doi.org/10.3389/fclim.2022.959229>.
- Le, D.M., Sørensen, H.R., Knudsen, N.O., Schjoerring, J.K., Meyer, A.S., 2014. Biorefining of wheat straw: accounting for the distribution of mineral elements in pretreated biomass by an extended pretreatment-severity equation. PMID: 25342972; PMCID: PMC4200199 *Biotechnol. Biofuels* 14 (1), 141. <https://doi.org/10.1186/s13068-014-0141-7>.
- Lefebvre, D., Goglio, P., Williams, A., Manning, D.A.C., de Azevedo, A.C., Bergmann, M., Meersmans, J., Smith, P., 2019. Assessing the potential of soil carbonation and enhanced weathering through Life Cycle Assessment: a case study for São Paulo State, Brazil. *J. Clean. Prod.* 233, 468–481.
- Lewis, A.L., Sakar, B., Wade, P., Kemp, S.J., Hodson, M.E., Taylor, L.L., Yeong, K.L., Davies, K., Nelson, P.N., Bird, M.I., Kantola, I.B., Masters, M.D., DeLucia, E., Leake, J.R., Banwart, S.A., Beerling, D.J., 2021. Effects of mineralogy, chemistry and physical properties of basalts on carbon capture potential and plant-nutrient element release via enhanced weathering. *Appl. Geochem.* 132, 105023.
- Liu, Z., Dreybrodt, W., Liu, H., 2011. Atmospheric CO<sub>2</sub> sink: Silicate weathering or carbonate weathering? *Appl. Geochem.* 26, S292–S294.
- Lothenbach, B., Kulik, D., Matschei, T., Balonis, M., Baquerizo, L., Dilnese, B.Z., Miron, D.G., Myers, R., 2019. Cemdata18: A Chemical Thermodynamic Database for Hydrated Portland Cements and Alkali-Activated Materials *Cement and Concrete Research*, vol. 115, pp. 472–506.
- McBride, M.B., Spiers, G., 2001. Trace element content of selected fertilizers and dairy manures as determined by ICP-MS. *Commun. Soil Sci. Plant Analysis* 32 (1&2), 139–156.
- McDonough, W.F., 1994. Chemical and isotopic systematics of continental lithospheric mantle. In: Meyer, H.O.A., Leonards, O. (Eds.), Kimberlites, Related Rocks and Mantle Xenoliths. Proceedings of the 5th International Kimberlite Conference, vol. 1. CPRM, Brasília, pp. 478–485.
- McKeith, B., 2004. Nutritional aspects of cereals. *Nutr. Bull.* 29, 111–142. <https://doi.org/10.1111/j.1467-3010.2004.00418.x>.
- Moosdorff, N., Renforth, P., Hartmann, J., 2014. Carbon dioxide efficiency of terrestrial enhanced weathering. *Env. Sci. Technol.* 48, 4809–4816.
- Morris, L.A., Nutter, W.L., Miller, W.P., Overcash, M., 2000. Treatment and use of pulp and paper and textile industry residues in southern U.S. forests. In: Henry, C.L., Harrison, R.B., Bastian, R.K. (Eds.), The Forest Alternative Principles and Practice of Residuals Reuse. Inov. Washington, Seattle, WA, U.S.A.
- Musci, G., Rácz, A., Mag, G., Antal, G., Csöke, B., 2019. Volume based closed-cycle Hardgrove grindability method. *Mining-Geol.-Pet. Bull.* 9–17 <https://doi.org/10.17794/rgn.2019.4.2.UDC:60.03>.
- Paces, T., 1983. Rate constants of dissolution derived from the measurements of mass balance in hydrological catchments. *Geochim. Cosmochim. Acta* 47, 1855–1863.
- Pade, C., Guimaraes, M., 2007. The CO<sub>2</sub> uptake of concrete in a 100 year perspective. *Cem. Con. Res.* 37, 1348–1356.
- Palandri, J.L., Kharaka, Y.K., 2004. In: Survey, U.S.G. (Ed.), A Compilation of Rate Parameters of Water-Mineral Interaction Kinetics for Application to Geochemical Modeling. U.S.
- Parkhurst, D.L., Appelo, C.A.J., 1999. User’s Guide to PHREEQC (version 2)—a Computer Program for speciation, batch-reaction, one-Dimensional transport, and Inverse geochemical calculations. U.S. Geological Survey, Water Resources Investigations Report 99-4259. Washington DC.
- Perrin, A.S., Probst, A., Probst, J.-L., 2008. Impact of nitrogenous fertilisers on carbonate dissolution in small agricultural catchments: implications for weathering CO<sub>2</sub> uptake at regional and global scales. *Geochim. et Cosmochim. Acta* 72, 3105–3123.
- Plaza, C., Zaccone, C., Sawicka, K., et al., 2018. Soil resources and element stocks in drylands to face global issues. *Sci Rep* 8, 13788. <https://doi.org/10.1038/s41598-018-32229-0>.
- Ren, J., et al., 2022. Pre-treatment of reclaimed concrete slurry waste for substituting cementitious materials: effect of treatment approach and substitution content. *J. Clean. Prod.* 380 (2), 134987.
- Renforth, P., 2012. The potential of enhanced weathering in the UK. *Int. J. Greenhouse Gas Cont.* 10, 229–243.
- Renforth, P., 2019. The negative emission potential of alkaline materials. *Nat Comm* 10, 1401. <https://doi.org/10.1038/s41467-019-09475-5>.
- Renforth, P., Henderson, G., 2017. Assessing ocean alkalinity for carbon sequestration. *Rev. Geophys.* 55, 636–674. <https://doi.org/10.1002/2016RG000533>.
- Renforth, P., Pogge von Strandmann, P.A.E., Henderson, G.M., 2015. The dissolution of olivine added to soil: implications for enhanced weathering. *Appl. Geochem.* 61, 109–118.
- Rosi-Marshall, E.J., Bernhardt, E.S., Buso, D.C., Driscoll, C.T., Likens, G.E., 2016. Acid rain mitigation experiment shifts a forested watershed from a net sink to a net source of nitrogen. *Proc. Natl. Acad. Sci. USA* 113, 7580–7583.
- Ruiz-Agudo, E., Kudlacz, K., Putnis, C.V., Putnis, A., Rodriguez-Navarro, C., 2013. Dissolution and carbonation of portlandite [Ca(OH)<sub>2</sub>] single crystals. *Environ. Sci. Technol.* 47, 11342. <https://doi.org/10.1021/es402061c>, 1134 dx.

- Russell, A., McDermott, F., McGrory, E., Cooper, M., Henry, T., Morrison, L., 2021. As–Co–Ni sulfarsenides in Palaeogene basaltic cone sheets as sources of groundwater arsenic contamination in co. Louth, Ireland. *Appl. Geochem.* 127, 104914.
- Shobana, S., Krishnaswamy, K., Sudha, V., Malleshi, N.G., Anjana, R.M., Palaniappan, L., et al., 2013. Finger millet (Ragi, *Eleusine coracana* L.): a review of its nutritional properties, processing, and plausible health benefits. *Adv. Food Nutr. Res.* 69, 1–39. <https://doi.org/10.1016/B978-0-12-410540-9.00001-6>.
- Spence, J., Telmer, K., 2005. The role of sulfur in chemical weathering and atmospheric CO<sub>2</sub> fluxes: evidence from major ions, δ<sup>13</sup>C<sub>DIC</sub>, and δ<sup>34</sup>S<sub>SO4</sub> in rivers of the Canadian Cordillera, 2005. *Geochem. Cosmochim. Acta* 69 (23), 5441–5458.
- Stets, E.G., Butman, D., McDonald, C.P., Stackpole, S.M., DeGrandpre, M.D., Striegl, R.G., 2017. Carbonate buffering and metabolic controls on carbon dioxide in rivers. *Global Biogeochem. Cycles* 31, 663–677. <https://doi.org/10.1002/2016GB005578>.
- Strelfer, J., Amann, T., Bauer, N., Kriegler, E., Hartmann, J., 2018. Potential and costs of carbon dioxide removal by enhanced weathering of rocks. *Environ. Res. Lett.* 13 <https://doi.org/10.1088/1748-9326/aaa9c4>.
- Taylor, L.L., Driscoll, C.T., Groffmann, P.M., Rau, G.H., Blum, J.D., Beerling, D.J., 2021. Increased carbon capture by a silicate-treated forested watershed affected by acid deposition. *Biogeosciences* 18, 169–188.
- ten Berge, H.F.M., van der Meer, H.G., Steenhuizen, J.W., Goedhart, P.W., Knops, P., et al., 2012. Olivine weathering in soil, and its effects on Growth and nutrient uptake in Ryegrass (*Lolium perenne* L.): a Pot experiment. *PLoS One* 7 (8), e42098. <https://doi.org/10.1371/journal.pone.0042098>.
- Trapote-Barreira, A., Cama, J., Soler, J.M., 2014. Dissolution kinetics of C–S–H gel: flow-through experiments. *Phys. Chem. Earth* 70–71, 17–31.
- Von Greve-Dierfeld, S., Lothenbach, B., Vollpracht, A., Wu, B., et al., 2020. Understanding the carbonation of concrete with supplementary cementitious materials: a critical review by RILEM TC 281-CCC. *Mater. Struct.* 136, 53–136.
- White, P.J., 2001. The pathways of calcium movement to the xylem. *J. Exp. Bot.* 52 (358), 891–899.
- White, A.F., Brantley, S.L., 2003. The effect of time on the weathering of silicate minerals: why do weathering rates differ in the laboratory and field? *Chem. Geol.* 202, 479–506.
- Wild, B., Daval, D., Beaulieu, E., Pierret, M.C., Viville, D., Imfeld, G., 2019. In-situ Dissolution Rates of Silicate Minerals and Associated Bacterial Communities in the Critical Zone.
- Xuan, D., Zhan, B., Poon, C.S., Zheng, W., 2016. Innovative reuse of concrete slurry waste from ready-mixed concrete plants in construction products. *J. Hazard. Mat.* 312, 65–72.
- Yi, W., Halliday, A.N., Alt, J.C., Lee, D.C., Rehkämper, M., Garcia, M.O., Langmuir, C.H., Su, Y., 2000. Cadmium, indium, tin, tellurium, and sulphur in oceanic basalt: implications for chalcophile element fractionation in the Earth. *J. Geophys. Res.* 105 (18), 927, 18,948.
- Zamanian, K., Pustovoytov, K., Kuzyakov, Y., 2016. Pedogenic carbonates: forms and formation processes. *Earth Sci. Rev.* 157, 1–17.
- Zheng, S., Liu, Z., Groves, C., 2022. Large-scale CO<sub>2</sub> removal by enhanced carbonate weathering from changes in land-use practices. *Earth Sci. Rev.* 225, 103915.